J Comput Neurosci (2008) 24:113–136
DOI 10.1007/s10827-007-0044-8

Spike-frequency adaptation generates intensity invariance in a primary auditory interneuron

Jan Benda · R. Matthias Hennig

Received: 4 October 2005 / Revised: 27 April 2007 / Accepted: 30 April 2007 / Published online: 30 May 2007

Abstract Adaptation of the spike-frequency response to constant stimulation, as observed on various timescales in many neurons, reflects high-pass filter properties of a neuron's transfer function. Adaptation in general, however, is not sufficient to make a neuron's response independent of the mean intensity of a sensory stimulus, since low frequency components of the stimulus are still transmitted, although with reduced gain. We here show, based on an analytically tractable model, that the response of a neuron is intensity invariant, if the fully adapted steady-state spike-frequency response to constant stimuli is independent of stimulus intensity. Electrophysiological recordings from the AN1, a primary auditory interneuron of crickets, show that for intensities above 60 dB SPL (sound pressure level) the AN1 adapted with a time-constant of ~ 40 ms to a steady-state firing rate of ~ 100 Hz. Using identical random amplitude-modulation stimuli we verified that the AN1's spike-frequency response is indeed invariant to the stimulus' mean intensity above 60 dB SPL. The transfer function of the AN1 is a band pass, resulting from a high-pass filter (cutoff frequency at 4 Hz) due to adaptation and a low-pass filter (100 Hz) determined by the steady-state spike frequency. Thus, fast spike-frequency adaptation can generate intensity invariance already at the first level of neural processing.

Keywords Spike-frequency adaptation · Invariance · Model · Auditory system · Cricket

Action Editor: Israel Nelken

J. Benda (✉)
Institute for Theoretical Biology, Biology Department,
Humboldt University, Invalidenstr. 43,
10115 Berlin, Germany
e-mail: j.benda@biologie.hu-berlin.de

R. Matthias Hennig
Behavioral Physiology, Biology Department,
Humboldt University, Invalidenstr. 43,
10115 Berlin, Germany

1 Introduction

Spike-frequency adaptation, a relaxation of an initially high spike-frequency to a lower steady-state level in response to a constant stimulus, is a common property of many neurons (Sobel and Tank 1994; Wang 1998; Sanchez-Vives et al. 2000; Fuhrmann et al. 2002; Gabbiani and Krapp 2006). The slow adaptation dynamics often acts subtractively on the input to the neuron, independent of the details of the underlying adaptation mechanism (Benda and Herz 2003). Subtractive adaptation adds a high-pass filter to the neuron's transfer function (Nelson et al. 1997; French et al. 2001; Benda et al. 2005). A high-pass filter attenuates slow stimulus components including the mean, whereas fast stimulus components are transmitted with high gain. Fast and slow stimulus components are distinguished by the cutoff frequency that is determined by the neuron's adaptation time-constant (Benda et al. 2005). If the slow stimulus components were suppressed completely, then the response to fast components will be independent of the mean intensity of the stimulus. Consequently, the response of such a neuron will be *intensity invariant*.

Intensity invariance is one step towards invariant object representations that are independent of, for example, mean intensity, contrast, position, or size (Barlow 1961; Laughlin 1989; Brenner et al. 2000; Wiskott 2003; Park et al. 2004; Gabbiani et al. 2004; Maravall et al. 2007). A well studied example is the invariance of the response of photo-receptors with respect to the mean illumination intensity that is achieved by an appropriate *shift* of the intensity–response curve (Laughlin 1989). This shift corresponds to the subtractive type of adaptation mentioned above. Likewise, the response of the motion sensitive H1-cell in the fly's visual system is contrast invariant, i.e. invariant with respect to changes of the motion variance, by appropriately changing the *slope* of the motion-response curve (Brenner et al. 2000; Fairhall et al. 2001).

Here we investigate spike-frequency adaptation and its role in creating intensity invariance in the auditory pathway of crickets. Crickets recognize their conspecific partners based on songs that last for minutes or even hours and that are composed of pulses and pauses in the range of tens of milliseconds (Huber et al. 1989; Hennig and Weber 1997). The behavioral context of this acoustic signal recognition task is well known from numerous psychophysical studies (Weber et al. 1981; Doolan and Pollack 1985; Hennig 2003). The intensity of the song varies depending on the distance between sender and receiver and neuronal correlates of song recognition in the cricket's brain are known to be intensity invariant (Schildberger 1984; see however Pollack and El-Feghaly 1993). In the auditory pathway of the cricket about 50 receptor afferents converge onto two ascending interneurons that project to the brain, of which the AN1 is most sensitive for conspecific songs (Esch et al. 1980; Wohlers and Huber 1982; Schildberger 1984; Hennig 1988). Compared to other sensory systems this auditory module exhibits a relatively simple topology which is dominated by feed-forward processing (Horseman and Huber 1994a; Huber et al. 1989).

First, we investigate intensity and contrast invariance of the spike-frequency response of the AN1 in response to random amplitude-modulated (RAM) stimuli. Then we analyze properties of spike-frequency adaptation of the AN1 by characterizing its onset, steady-state and adapted intensity-response curves, as well as the adaptation time-constant. We summarize our results in a phenomenological model that is solely based on the measured time constant and intensity-response curves of the adaptation process. The model successfully predicts the response to RAM stimuli at different intensities and thus supports the causal link between spike-frequency adaptation and the observed intensity invariance. Finally, we discuss the components of the AN1's transfer function due to adaptation and spike generation.

2 Materials and methods

2.1 Preparation

Laboratory-reared crickets of the species *Teleogryllus oceanicus* were used in all experiments. Both pairs of wings as well as the meso- and metathoracic legs were removed and the animal was fixed ventral side up to a small platform. The prothoracic legs with the ears were waxed to pins at the coxae and the tarsi in a normal walking position. Ascending and descending connectives from the prothoracic ganglion were cut in order to reduce neuronal background activity. See Hennig (1988) for a more detailed description.

2.2 Recordings and stimulation

Dual extracellular hook-electrode recordings were made from the connectives between the prothoracic and subesophageal ganglia that contain the axons of AN1. The electrodes were electrically isolated with a vaseline–mineral oil mixture and the signal was amplified in differential mode. The voltage trace (Fig. 1(a)) was digitized with an AD-board (AT-MIO-16E-1, 12 bit, National instruments, Austin, TX) at 20 kHz sampling rate and stored on disk.

The AN1 is a small neuron in the connective, which contains axons of more than 1,000 mostly non-auditory cells. In the hook-electrode recordings only two units, the AN1 and the AN2, responding to auditory stimuli are present (Fig. 1(a)). The peak amplitudes of the AN1 spikes were well separable from the background noise by applying an amplitude window (Fig. 1(b)). The identity of the AN1 spikes was further established by comparing physiological properties of the extracellularly recorded unit with those of the AN1, as established by intracellular recordings by Hennig (1988). Low thresholds below 55 dB SPL and high copying fidelity of pulsed tones clearly distinguished the AN1 from the AN2 at low carrier frequencies of 4.5 kHz (Wohlers and Huber 1982; Hennig 1988). We used Labview software (National Instruments, Austin, TX) for offline detection of spikes.

Often we observed a peak in the interspike interval histograms below 2 ms (Fig. 1(c)). This peak likely corresponds to a few false-positive spikes originating from other neurons. Therefore we discarded spikes less than 2.9 ms apart from the preceding spike for the

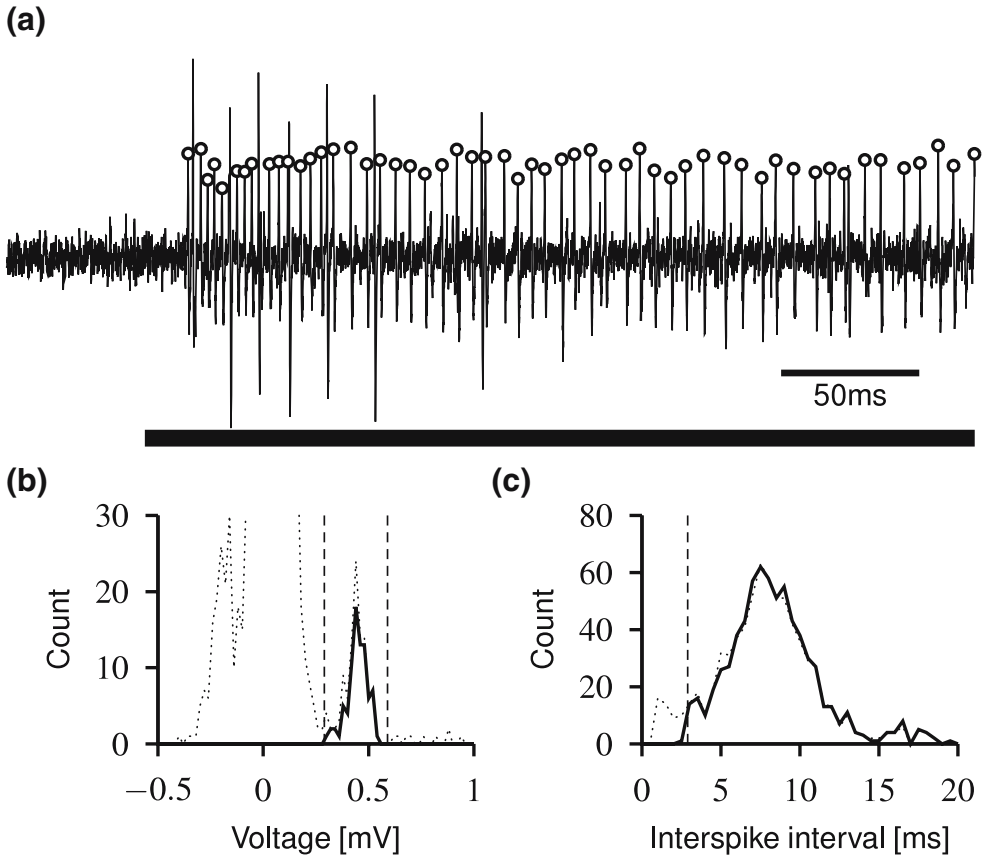

Fig. 1 Recording and detection of AN1 spikes. (**a**) An example of a recording trace that we obtained by stimulation with a 4.5 kHz tone at 80 dB SPL (*black bar*). The *open circles* mark the peaks of the spikes that we detected as AN1 spikes. The few larger spikes at the beginning of the voltage trace originate from the AN2. (**b**) A histogram of all local maxima (*dotted line*) in the trace shown in (**a**). The large peak around zero (truncated, maximum count is 383) is baseline noise including many non-auditory units. The peak voltages of the AN1 spikes (*solid line*) form a peak in the histogram that is well separated from the baseline noise as well as the AN2 spikes. The vertical dashed lines mark the thresholds we used for detecting AN1 spikes. (**c**) An interspike-interval histogram (*dotted line*) compiled from the steady-state response (between 250 and 500 ms after stimulus onset) to 25 repetitions of a constant amplitude stimulus with 80 dB SPL and 500 ms duration. We discarded all spikes less than 2.9 ms apart from the previous spikes (*vertical line*), since they introduced an additional peak in most interspike-interval histograms at between 1 and 2 ms. The *solid line* is the histogram of the remaining spikes that we used for further analysis

subsequent analysis of spike frequencies (Schildberger 1984). Reanalyzing our data using a value of 2 ms did not significantly change our results. Only at high intensities the activity of the AN2—another ascending auditory interneuron—may have masked the AN1 activity with its larger spikes (large spikes in Fig. 1(a)). The AN2 responded transiently to stimuli above 80 dB SPL (decibel sound-pressure level) which may have partly caused the reduction of the onset response of the AN1 at intensities above 80 dB SPL visible in Fig. 6(a).

The extracellular recordings avoid damage to the neuron as may be the case with intracellular recordings. In addition, stable recordings allowed to run the whole stimulus protocol for this study, which lasted about one and a half hours. These advantages of the extracellular recordings clearly outweighed the few additional and missed spikes, since for our analysis spike frequency and not the exact spike timing was most important.

Data from 13 AN1 neurons from 13 crickets (one male, twelve females, there is no evidence for sex-specific differences at this level of processing; Hennig 1988) were included in our analysis. Eleven other recordings were excluded since either the background activity of the recording was above 57 Hz (note, that the background activity results mostly from false positives in the spike detection and not from spontaneous activity), the threshold of the two onset f-I-curves (spike frequency versus intensity) measured at the beginning and the end of an experiment differed by more than 8 dB, or their threshold was above 55 dB SPL.

The recording setup was lined with sound-absorbing foam to reduce echoes. Free-field acoustic stimuli were

presented at the input side of the AN1 by a dynamical loudspeaker at a distance of 34 cm. All stimuli used in this study are amplitude modulations of a 4.5 kHz tone, which corresponds to the carrier frequency of the calling song of *T. oceanicus* and is at the same time the best frequency of the AN1 (Hennig 1988). The stimulus envelope was multiplied analogically with the carrier sine-wave. All constant amplitude and pulse-modulated stimuli had rise and fall times of 2 ms.

The single-cell data shown in Figs. 2, 4–9 and 11 were all obtained from the same cell to allow comparisons of its responses to various stimuli with its f-I curves. The response properties of this neuron were close to the averaged results as for example summarized in Table 1. Figure 10(a–c) shows data from a different cell for comparison.

2.3 Onset and steady-state f-I curves

The onset and steady-state f-I-curves, $f_0(I)$ and $f_\infty(I)$, are important for characterizing spike-frequency adaptation (Benda and Herz 2003). Both f-I-curves were measured at the beginning and at the end of an experiment. Tones with constant amplitude of 500 ms duration were applied at intensities ranging from 30 to 93 dB SPL with 3 dB increment. Each stimulus was repeated 25 times, the pauses between the stimuli were 1.5 s long, i.e. three times the duration of the preceding stimulus. The time course of the spike frequency was calculated for every millisecond as the trial-averaged inverse of the interspike intervals that contain that particular time. After smoothing the spike frequency with a rectangular 3 ms averaging window, the maxima within the first 100 ms after stimulus onset were used for the onset f-I-curve. For the steady-state f-I-curve the mean spike frequencies from 300 to 450 ms after stimulus onset were calculated.

For a parameterization of the resulting f-I-curves we fitted a Boltzmann function

$$f(I) = \frac{f^{\max} - f^{\min}}{1 + \exp(-k(I - I^0))} + f^{\min} . \tag{1}$$

to the data. The Boltzmann function is a sigmoidal function that raises around I^0 linearly from its minimum value $f^{\min}$ to its maximum value $f^{\max}$ (see Fig. 6(b) for illustration). It reaches half its height at I^0 where it is well approximated by a straight line with slope

$$\text{slope} = s = (f^{\max} - f^{\min})k/4 . \tag{2}$$

We define the threshold of an f-I curve as the stimulus intensity where the tangent of the corresponding Boltzmann function at I^0 intersects $f^{\min}$:

$$\text{threshold} = I^{\text{th}} = I^0 - 2/k . \tag{3}$$

Finally, the width of the dynamical range is the intersection of the tangent with $f^{\max}$ minus the threshold:

$$\text{width} = 4/k . \tag{4}$$

For the steady-state f-I curve we first estimated all four parameters, $f_\infty^{\min}$, $f_\infty^{\max}$, I_∞^0 and k_∞, from the data and then refined them by a fit of the Boltzmann function to the data using a simplex algorithm (Press et al. 1992). For the onset f-I curve we set $f_0^{\min}$ to $f_\infty^{\min}$ and obtained the remaining three parameters, $f_0^{\max}$, I_0^0 and k_0, from a fit of the Boltzmann function to the data.

We determined the effective time constant of spike-frequency adaptation by fitting a single exponential function

$$f(t) = (f_0 - f_\infty)\exp(-t/\tau_{\text{eff}}) + f_\infty \tag{5}$$

to the spike-frequency response evoked by constant amplitude stimuli using the Levenberg–Marquardt algorithm (Press et al. 1992). The onset and steady-state spike frequencies, f_0 and f_∞, were determined as described above.

2.4 Adapted f-I curves

Adapted f-I-curves were obtained by first adapting the neuron for 500 ms to a tone with constant amplitude and given background intensity I_b. The onset response to a different intensity was tested by a subsequent 100 ms test-stimulus and then the cell was adapted back to I_b during the following 300 ms (Fig. 7(a), lower panel). This was repeated for 12 different test intensities spaced by 3 dB.

The inter-stimulus interval of 300 ms was chosen to be about five times the effective time constant of adaptation (on average 62 ms, see Section 3)—long enough to allow the cell to adapt back to I_b. The specific alternating order of the intensities of the test pulses turned out to result in the most stable steady-state spike frequency in response to the background intensity and thus a fixed adaptation strength directly before each test pulse. Especially, the effects of adaptation processes with longer time constants are minimized with this balanced ordering of intensities. A randomized order of intensities, for example, would allow several high intensities in a row that are then more likely to activate adaptation processes slower than the one we are investigating.

Five background intensities were used: $I_b = 35$, 47, 59, 71 and 83 dB SPL. The onset response of the neuron adapted to I_b was determined as the largest deviation of the spike-frequency after onset of the test-stimulus from the spike frequency averaged over 50 ms before the test-stimulus. Before measuring the onset response the spike-frequency was smoothed with a 3 ms wide rectangular window and only extrema between 12 and 62 ms after onset of the test-stimuli were considered in order to account for the latency of the response (Hennig 1988). Again, we used the Boltzmann function (1) for a parameterization of the adapted f-I-curves. We estimated all four parameters, $f_a^{\min}$, $f_a^{\max}$, I_a^0 and k_a, from the data and then refined them by a fit of the Boltzmann function to the data using a simplex algorithm (Press et al. 1992).

2.5 RAM and pulse AM stimuli

In order to test for intensity invariance as well as the adaptation model, we recorded the responses to different random amplitude-modulated (RAM) and pulse amplitude-modulated (AM) stimuli. The carrier frequency for both types of stimuli was 4.5 kHz. Each stimulus was repeated 25 times. The envelope of the eight different RAM stimuli had a flat power spectrum upto cutoff frequencies of 50, 100, 200 and 400 Hz, standard deviations of 4 and 6 dB, and a duration of 1000 ms. They were first presented at 80 dB SPL and then at 90 and 70 dB SPL (peak intensities, which is three times the standard deviation of the stimuli above their mean).

All pulse AM stimuli had a duty cycle of 50% (duration of the pulses as compared to the period), were about 500 ms long and were presented at 80 dB SPL. The durations of pulses and pauses used were 5, 8, 10, 15, 20, 30, 40, and 60 ms and covered the behaviorally relevant range (Hennig 2003).

The time course of the spike frequency in response to the RAM and pulse AM stimuli was calculated for every millisecond as the trial-averaged inverse of the interspike intervals that contain that particular time. The spike frequency was smoothed with a rectangular 3 ms averaging window.

From the spike-frequency response $r(t)$ to the RAM stimuli $s(t)$ we computed the gain according to

$$g(\omega) = \left| \frac{\langle R(\omega) S^*(\omega) \rangle}{\langle S(\omega) S^*(\omega) \rangle} \right| \tag{6}$$

where $R(\omega)$ and $S(\omega)$ are the fourier transformations of $r(t)$ and $s(t)$, respectively, as a function of angular frequency $\omega = 2\pi f_c$ of the frequency f_c, S^* is the complex conjugate of S, and $|\cdot|$ is the magnitude of the complex argument. The angled brackets denote averaging over 256 ms (256 data points) wide, overlapping, and Bartlett-windowed, segments of data. Note, that the RAM stimuli were designed for testing the model performance and are rather too short for a good spectral analysis. In particular, they are of limited use to obtain reliable estimates of the response-to-response coherence (Marsat and Pollack 2005).

2.6 Model predictions

Based on the f-I curves we constructed a phenomenological model for the spike-frequency response of the AN1 (see Section 3). The model is completely defined by the f-I curves measured for each cell. However, the steep slope of the onset f-I curve make the quality of the model predictions very vulnerable to small errors in the position of this f-I curve. Since the sensitivity of the AN1 shows small variations during a recording we monitored the onset f-I curve throughout the recording 7 times (median, range: 1–10) using stimuli as for the adapted f-I curves described above with the background amplitude set to 0 and the initial adaptation stimulus removed. For the model predictions we then used the onset f-I curve that was measured temporally closest to the stimulus in question.

We integrated the model (9) using the Euler method with a time step of 0.05 ms and initial conditions $f(t = 0) = 0$ and $A(t = 0) = 0$).

3 Results

3.1 Intensity invariance of the AN1 response

In order to test the response properties of the cricket's AN1 neuron for intensity invariance we used random amplitude-modulations (RAMs) as dynamical stimuli with four different cutoff frequencies (50, 100, 200 and 400 Hz) and two different standard deviations (4 and 6 dB). Each RAM stimulus was presented at three different mean intensities. A "low" intensity ($\bar{I} =$ 52 dB SPL) slightly above the threshold of the AN1, a "medium" intensity ($\bar{I} = 62$ dB SPL), and a "high" intensity ($\bar{I} = 72$ dB SPL). Note that changing the intensity of a sound stimulus corresponds to a multiplication of the sound pressure wave with a constant factor. However, the standard deviation of the amplitude modulation stimuli measured in decibel is not affected by changing the sound intensity, since decibel is a logarithmic measure of sound pressure.

A direct comparison of the response to the same RAM presented at the three different intensities

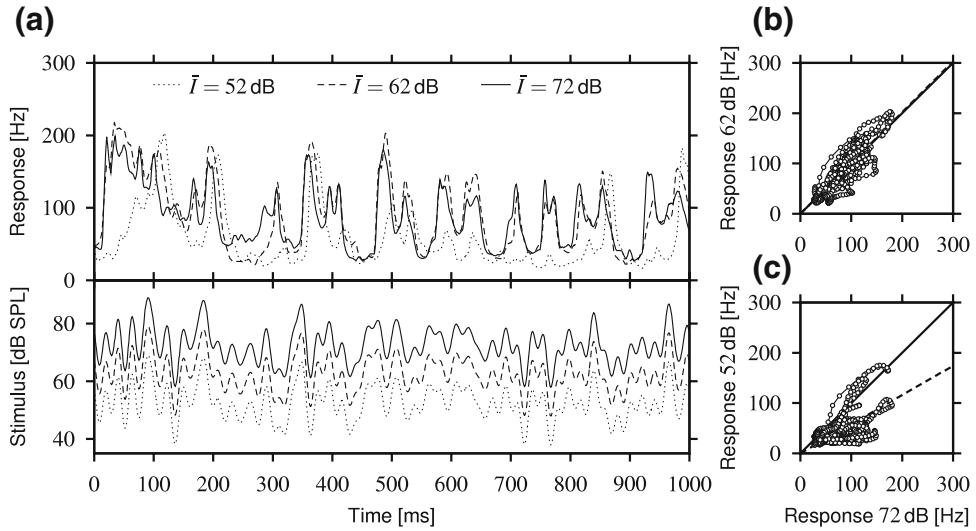

Fig. 2 Intensity invariance of the spike-frequency response of the AN1. (**a**) The spike-frequency responses (*upper panel*) to stimulation with RAM stimuli (*lower panel*; cutoff frequency 50 Hz, standard deviation 6 dB) at three different mean intensities of $\bar{I} = 52$, 62, and 72 dB SPL as indicated. (**b**) Comparison of the spike-frequency responses to the RAM stimuli with mean intensity of $\bar{I} = 62$ dB SPL and $\bar{I} = 72$ dB SPL between 250 and 950 ms after stimulus onset. First, to account for different response delays, we shifted the spike-frequency traces relative to each other such that the correlation coefficient between them was maximized (see also Fig. 3(c) and Section 2). Each point in the graph then represents the spike frequencies of the responses to the two stimuli at corresponding times. The high correlation coefficient ($r = 0.88$) and a slope of 1.01 of the regression line (*dashed line*) show that the responses are virtually identical. (**c**) The response to the stimulus at $\bar{I} = 52$ dB SPL was smaller (slope of regression line (*dashed line*) is 0.58) than the one to $\bar{I} = 72$ dB SPL, but the two are still correlated ($r = 0.59$). The data points on the identity line are mainly due to the peaks in the response at about 370 and 860 ms, where the responses to both intensities are similar

is shown in Fig. 2(a). The responses evoked by the medium- and high-intensity stimuli were almost identical whereas the low-intensity response differed from the other responses.

In Fig. 2(b,c) the spike-frequency responses to the medium- and low-intensity stimuli are plotted against the response to the high-intensity stimulus for times between 250 and 950 ms after stimulus onset. We excluded the initial 250 ms of the response from the analysis since there the response seemed to adapt strongly. This adaptation is treated separately below.

The responses to the two higher intensities were highly correlated (Fig. 2(b), $r = 0.88$) and the slope of the corresponding regression line was 1.01. The response to the low-intensity stimulus, however, matched the responses to the louder stimuli less well. The responses to the low- and high-intensity stimulus were still correlated ($r = 0.59$) but the slope of the regression line was reduced to 0.58 (Fig. 2(c)).

The results of a detailed quantification of intensity-invariance from all cells are summarized in Fig. 3. We computed several measures from the responses to the RAM stimuli between 250 and 950 ms after stimulus onset. The mean firing rates (Fig. 3(a)) generated by stimuli with medium and high intensities were similar (but still significantly different: 98 ± 17 Hz and 104 ± 17 Hz, respectively), whereas the low intensity stimuli evoked smaller mean firing rates (71 ± 15 Hz). The average modulation depth of the spike-frequency response, measured as its standard deviation (Fig. 3(b)), ranged between 22 and 28 Hz. The modulation depth of the response to the high-intensity stimuli (22 ± 8 Hz) was significantly smaller than the one to the medium-intensity stimuli (27 ± 9 Hz).

For a comparison of pairs of spike-frequency responses to the same stimulus at two different intensities we first shifted the responses relative to each other such that the correlation between them was maximized, in order to account for different response delays (as in Fig. 2(b,c)). On average, the responses to the low intensity stimuli were delayed by 8.4 ± 3.7 ms relative to the responses to the high intensity stimuli (Fig. 3(c)). The responses to the medium-intensity stimuli were delayed by only 3.4 ± 1.6 ms.

The root-mean-squared (rms) difference between spike-frequency traces was higher for comparisons of low-intensity stimuli with high-intensity stimuli (25 ± 6 Hz) than for comparisons between medium- and high-intensity stimuli (18 ± 4 Hz, Fig. 3(d)). The values of the rms differences of the responses were almost of the same magnitude as the standard deviation of the spike-frequency responses (Fig. 3(b)). However, a closer look

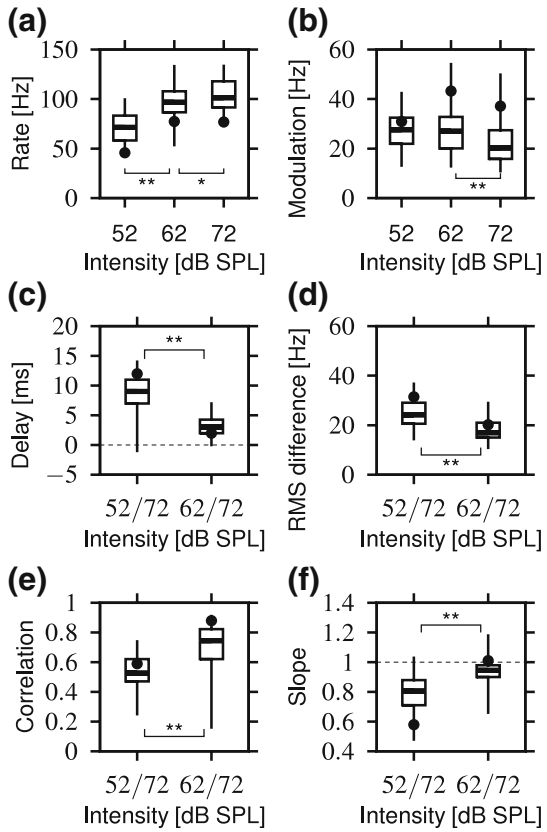

Fig. 3 Measures of intensity invariance. (**a**) Dependence of the mean firing rate on the mean intensity of the RAM stimuli. (**b**) The modulation depth computed as the standard deviation of the spike-frequency response. (**c**) The delays that were necessary to maximize the correlation between the spike-frequency responses. Positive delays indicate that the original response of the low- and medium-intensity stimuli was delayed relative to the response of the high-intensity stimuli. The data in the following panels were evaluated for the delayed responses. (**d**) The root–mean–squared difference between pairs of spike-frequency responses for the same stimulus at two different intensities (52 and 72 dB SPL, 62 and 72 dB SPL). (**e**) The correlation coefficient between pairs of spike-frequency responses. (**f**) The slopes of the corresponding regression lines. All measures were computed between 250 and 950 ms after onset of the stimulus (RAM stimuli with cutoff frequencies 50, 100, 200, or 400 Hz and standard deviations 4 or 6 dB). In each of twelve cells all eight different stimuli were presented with a mean intensity of 62 and 72 dB SPL ($n = 96$). In five cells we presented in addition all stimuli at 52 dB SPL ($n = 40$). Values are medians (*thick line*) with 1. and 3. quartile (*box*) and minimum and maximum value (*whiskers*). The dots present the values from the example shown in Fig. 2. Asterisks indicate significant differences obtained from a two-tailed Wilcoxon test applied to the data from the five cells where all three intensities where measured (* $p = 0.03$, ** $p \ll 0.001$, $n = 40$)

at the raw traces reveals that the responses to the medium- and high-intensity stimuli quickly rise and fall between the minimum and maximum spike frequency (Fig. 2(a)). Consequently, small differences in the exact timing of those deflections, as they are visible in Fig. 2(a), introduce very large differences (more than 100 Hz) for many but brief time periods that add up to relatively high rms differences. The same effect also deteriorates the correlation coefficient (Fig. 3(e)).

The correlation coefficients between the responses were higher between medium- and high-intensity stimuli ($r = 0.71 \pm 0.14$) than between low- and high-intensity stimuli ($r = 0.53 \pm 0.12$, Fig. 3(e)). The slopes of the corresponding regression lines were close to one (0.94 ± 0.07) between medium- and high-intensity stimuli, but smaller between low- and high-intensity stimuli (0.79 ± 0.13, Fig. 3(f)).

In summary, responses to medium- and high-intensity stimuli were very similar as indicated by their almost identical mean firing rate, low rms differences, high correlation coefficients, and slopes of the corresponding regression lines close to one. However, the responses were not identical since their modulation depth was somewhat reduced in response to high-intensity stimuli and as a consequence the slopes of the regression lines were slightly below one. For low-intensity stimuli the similarity to the responses to stimuli with higher intensities was significantly reduced as indicated by higher rms differences, and correlation coefficients of about 0.5. Thus, the response of the AN1 is approximately intensity invariant for mean-intensities of the stimuli above about 60 dB SPL.

3.2 Intensity-invariance versus contrast-invariance

Another fundamental type of invariance that may be computed during peripheral sensory processing is contrast invariance. The response of a neuron evoked by a sensory stimulus is contrast-invariant if this response is independent of the contrast, i.e. the variance or standard deviation, of the stimulus.

In order to test whether the AN1's response is contrast invariant, we first plotted spike frequency against the corresponding intensity of a RAM stimulus at each millisecond (open circles in Fig. 4(a), right panel). We then divided the intensity axis into 3 dB wide bins and averaged the spike frequencies in each of the stimulus-intensity bins. This procedure resulted in an intensity-response curve as displayed in Fig. 4(a). The same stimulus with a higher mean intensity shifts this intensity-response curve by the intensity difference along the intensity axis (Fig. 4(b)), as predicted from our previous results for an intensity-invariant response.

On the other hand, if the response was contrast-invariant, then RAM stimuli with different standard deviations should scale the slope of the intensity–response curve by their relative standard deviations (Brenner et al. 2000; Maravall et al. 2007). Consequently, if the

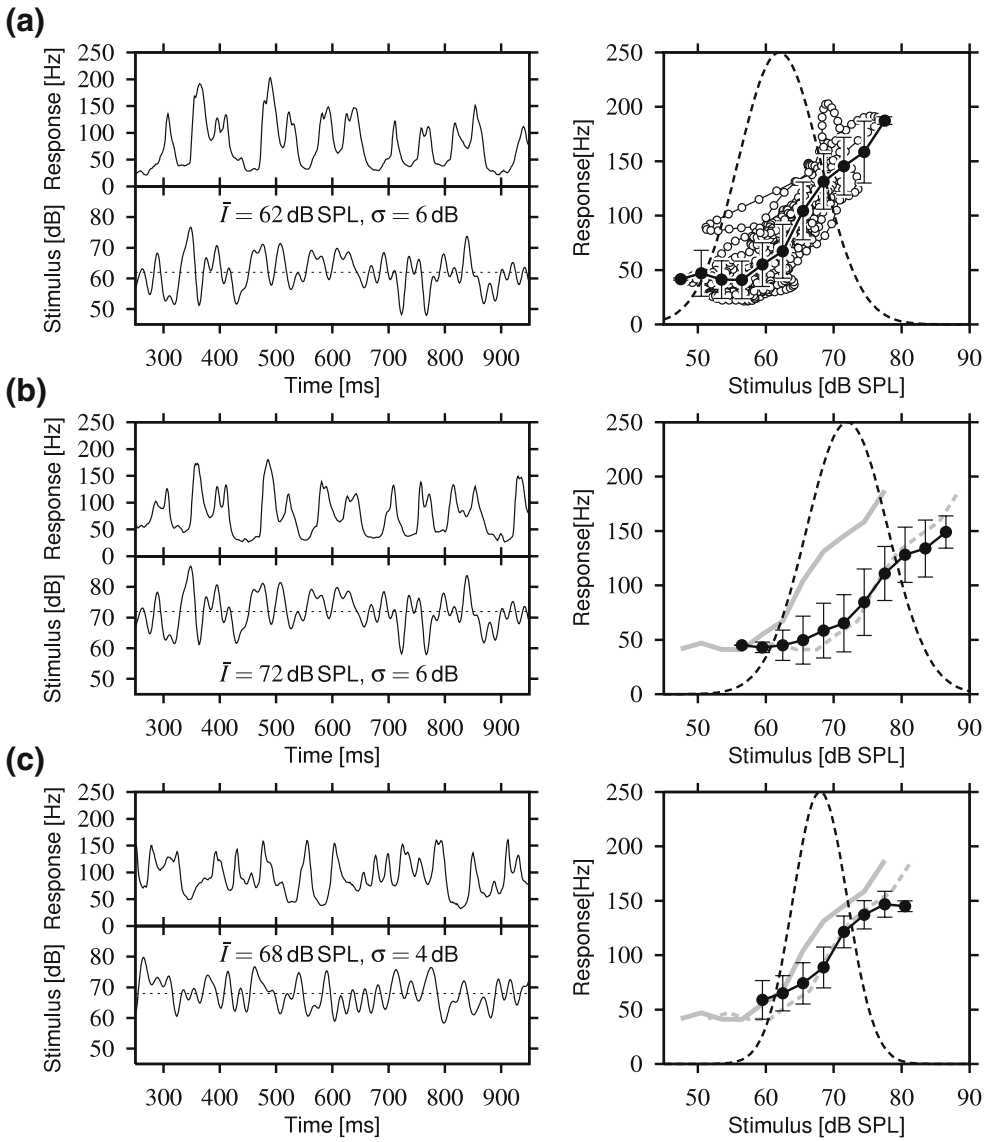

Fig. 4 Intensity invariance and contrast invariance. The spike-frequency responses (*upper panels*) between 250 and 950 ms after stimulus onset evoked by RAM stimuli (*lower panels*, cutoff-frequency 50 Hz) with different mean intensities $\bar{I}$ and standard deviations σ as indicated are shown in the *left column*. In the *right column* the corresponding intensity-response curves (*filled circles*, mean with standard deviation) obtained by binning and averaging the spike-frequency response (*upper left panel*, see text for details) plotted against the stimulus (*lower left panel*) (*open circles* in (**a**)), together with the amplitude distribution of the stimuli (*dashed lines*) are displayed. The intensity-response curve from (**a**) is replotted in (**b**) and (**c**) as a reference (*gray solid line*) and additionally shifted on top of the intensity–response curves (*gray dashed line*) for comparison. (**a**) The response to the reference stimulus with standard deviation $\sigma = 6$ dB at $\bar{I} = 62$ dB SPL. (**b**) The same stimulus as in (**a**), but with a 10 dB higher intensity, evokes a very similar response. The intensity-response curve is shifted to higher intensities. (**c**) A stimulus with a smaller standard deviation ($\sigma = 4$ dB SPL) does not increase the slope of the intensity-response curve, although the amplitude distribution is narrower

standard deviation of the stimulus is decreased, the slope of the intensity-response curve should become steeper in order to match the amplitude distribution better. However, this is clearly not the case for the AN1, as Fig. 4(c) demonstrates. The intensity-response curves computed from the data recorded in the other eleven cells had the same properties as the ones shown in Fig. 4. Thus, the response of the AN1 is not contrast-invariant.

3.3 Spike-frequency adaptation of the AN1

In the following we first investigate spike-frequency adaptation that is obvious during the first few hundreds

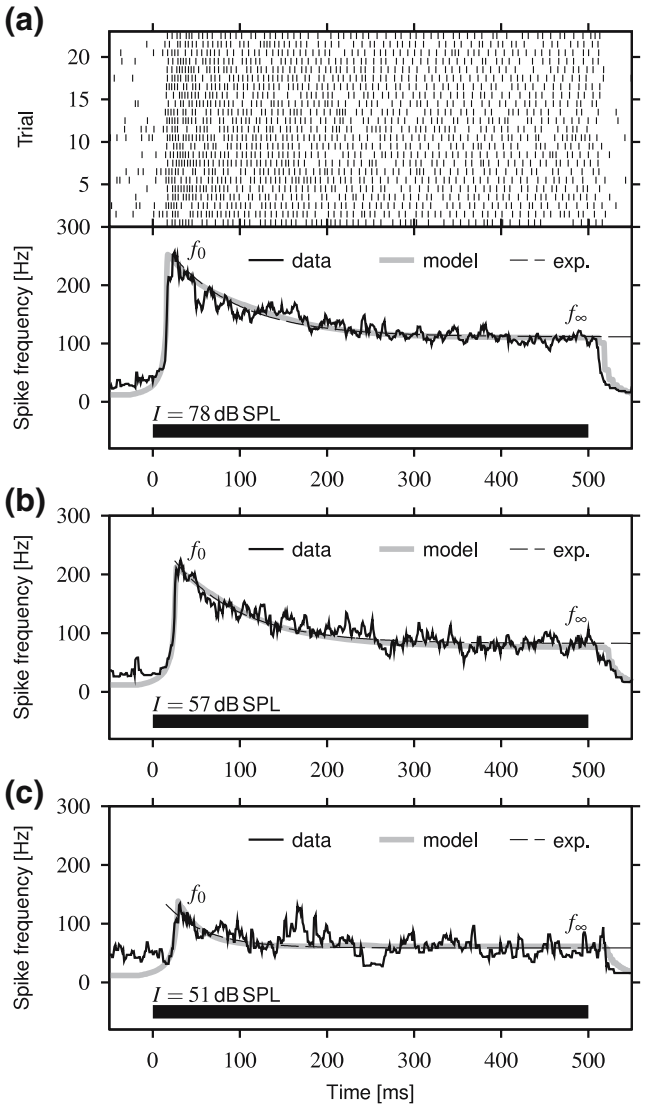

Fig. 5 Spike-frequency adaptation to stimuli with constant amplitude. (**a**) The response to a 78 dB SPL stimulus switched on at $t = 0$ (indicated by the *black bar* in the *lower panel*). The *upper panel* shows the individual spike responses for 23 trials. In the *lower panel* the corresponding time course of the spike frequency (*solid line*) is compared with the fit of the model ((9), *gray line*) and the fit with a single exponential function ((5), *dashed line*, mostly on top of the *gray line*). (**b**) and (**c**) Same as in (**a**) for lower stimulus intensities I as indicated

of milliseconds after stimulus onset (Fig. 5) in detail. We then link the properties of the observed spike-frequency adaptation with the intensity invariance described above (Figs. 2, 3, and 4) by means of a model.

Stimulation of the cricket's auditory system with sinusoidal tones of constant amplitudes evoked a spike-frequency response in the AN1 that adapted from an initial response f_0 down to a steady-state response f_∞ within a few hundreds milliseconds. Typical examples of such an experiment with different intensities of the stimulating tone are displayed in Fig. 5.

3.4 Onset and steady-state f-I curves

After a sufficiently long absence of any stimulus a cell completely recovers from adaptation and is in its unadapted state. In this case, the onset response f_0, i.e. the initial higher spike frequency directly after the onset of a stimulus, for different stimulus intensities I measures the onset f-I (spike-frequency versus intensity) curve $f_0(I)$ that characterizes the response properties of the non-adapted neuron (Figs. 5 and 6(a)).

The spike-frequency response to the constant amplitude stimuli decays down to the steady-state responses f_∞ that define the steady-state f-I curve $f_\infty(I)$. The steady-state f-I curve determines the spike-frequency response evoked by "slow" stimuli that change on timescales much longer than the adaptation time-constant. Furthermore, the difference between the onset and the steady-state f-I curve contains information about the maximum adaptation strength in dependence of stimulus intensity and/or spike frequency (Benda and Herz 2003).

We determined the onset as well as steady-state f-I curves of the AN1 from the responses to 500 ms long constant amplitude stimuli. Examples of the time course of the spike frequency evoked by such stimuli with different intensities are shown in Fig. 5 and the resulting f-I curves are displayed in Fig. 6(a). We parameterized the f-I curves with Boltzmann functions ((1), Fig. 6(b)), that describe the data sufficiently well.

Properties of the f-I curves averaged over all 13 cells (two f-I curve measurements per cell) are summarized in Table 1. On average, the threshold of both the onset and the steady-state f-I curve is at about 40 dB SPL. The steady-state f-I curve then monotonically increases to its saturation level at on average 114 Hz, about half the maximum spike frequency of the onset f-I curve. Above about 60 dB SPL the steady-state f-I curve is approximately flat up to the highest intensity we measured (93 dB SPL).

3.5 Adapted f-I curves

In order to investigate how the response properties of the neuron depend on the adaptation strength we measured adapted f-I curves. We first adapted the cell to a certain adaptation strength by a constant amplitude stimulus with intensity I_b. By subsequent test stimuli of 100 ms duration and various intensities we probed the onset response of the cell adapted to I_b (Fig. 7(a)). After each test stimulus the cell was adapted back to the background intensity for 300 ms. We measured the onset responses to the test stimuli as the largest deviation from the spike frequency averaged over 50 ms

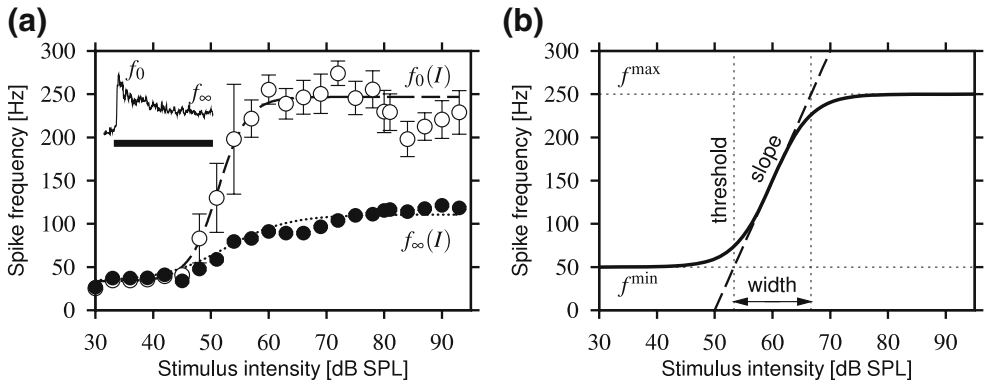

Fig. 6 Intensity-response curves (f-I curves). (**a**) The onset ($f_0(I)$, *open circles*) and steady-state f-I curve ($f_\infty(I)$, *filled circles*) as obtained from responses to constant amplitude stimuli (*inset* and Fig. 5). The *error bars* indicate the standard error. The *dashed* and the *dotted line* are Boltzmann functions (1) fitted to the data. See Section 2 for the reduction of onset responses at intensities above 80 dB SPL. (**b**) Parameters of a Boltzmann function (1) (*solid line*) describing an f-I curve: Minimum f^{min} and maximum f^{max} spike frequency, slope (2), threshold (3), and width (4). The tangent at I^0 (*dashed line*, here $I^0 = 60$ dB SPL) is a good approximation of the dynamical range. The f-I curves shown in (**a**) have the following values: onset f-I curve $f_0^{min} = 34$ Hz, $f_0^{max} = 245$ Hz, slope= 21 Hz/dB, threshold= 46 dB, width= 10 dB, steady-state f-I curve $f_\infty^{min} = 34$ Hz, $f_\infty^{max} = 111$ Hz, slope= 3.6 Hz/dB, threshold= 42 dB, width= 22 dB

just before these stimuli, and used them to construct adapted f-I curves (Fig. 7(b)).

The adapted f-I curves were well fitted by the Boltzmann function ((1), χ^2-test $p = 0.82 \pm 0.35$, $n = 58$). Adaptation obviously shifted the f-I curves along the intensity axis (Fig. 7(b,c)). The thresholds of the adapted f-I curves defined by Eq. (3) as a measure of their position were well correlated with the adaptation stimulus I_b: $r = 0.98 \pm 0.01$, $n = 13$ cells, $p < 0.03$ (Fig. 7(d)). The maximum shifts (threshold intensity of the adapted f-I curve minus the threshold of the onset f-I curve) ranged from 18 up to 38 dB. In the following we define this adaptation induced shift of the thresholds of the f-I curves as the adaptation strength A.

The shift of the adapted f-I curves was accompanied by a significant reduction of the maximum spike frequency f_a^{max} (Fig. 7(c)). The correlation coefficient between the relative maximum spike frequency f_a^{max}/f_0^{max} and the shift A was on average $r = -0.83 \pm 0.25$ and is significant with $p < 0.05$ in 8 out of 13 cells (Fig. 7(e)). However, the slopes (2) of the adapted f-I curves were not correlated with the shift ($r = 0.06 \pm 0.34$, $n = 13$ cells, $p = 0.71 \pm 0.23$).

The relationship between the reduction in maximum spike frequency and the adaptation strength is illustrated in Fig. 7(f), where we plotted the relative reduction

$$\alpha = (f_a^{max} - f_a^{min})/(f_0^{max} - f_0^{min}) \tag{7}$$

as a function of A. Visual inspection of such plots showed that the initial decrease of α with A was linear in most cases. On the other hand, for strong adaptation (large A) α should asymptotically reach the maximum spike frequency of the steady-state f-I curve relative to the onset f-I curve $r = (f_\infty^{max} - f_\infty^{min})/(f_0^{max} - f_0^{min})$. We therefore decided to use a modified Boltzmann function for a phenomenological description of the dependence of α on A:

$$\alpha(A) = r + 2\frac{1-r}{1+\exp(\gamma A)} \,. \tag{8}$$

Table 1 Properties of the f-I curves of the AN1 (mean with standard deviation)

f-I curve	f^{min} (1) Hz	f^{max} (1) Hz	Slope (1) Hz/dB	Width (1) dB	Threshold (1) dB SPL	χ^2-test (2) p
Onset $f_0(I)$	38 ± 12 (3)	214 ± 20	16 ± 6	12 ± 4	43 ± 6 (4)	0.98 ± 0.04
Steady-state $f_\infty(I)$	38 ± 12	114 ± 19	3.4 ± 1.1	25 ± 11	40 ± 8 (4)	0.90 ± 0.24

(1) See Fig. 6(b) and Eqs. (2), (3), and (4) in the Section 2 for definitions.
(2) Probability of getting a χ^2 value at least as high as the observed one for the Boltzmann function (1).
(3) Minimum frequency of onset f-I curves was set to the value of the corresponding steady-state f-I curve.
(4) Thresholds are not significantly different (t-test, $t = 1.51$, $p = 0.14$, $n = 26$).

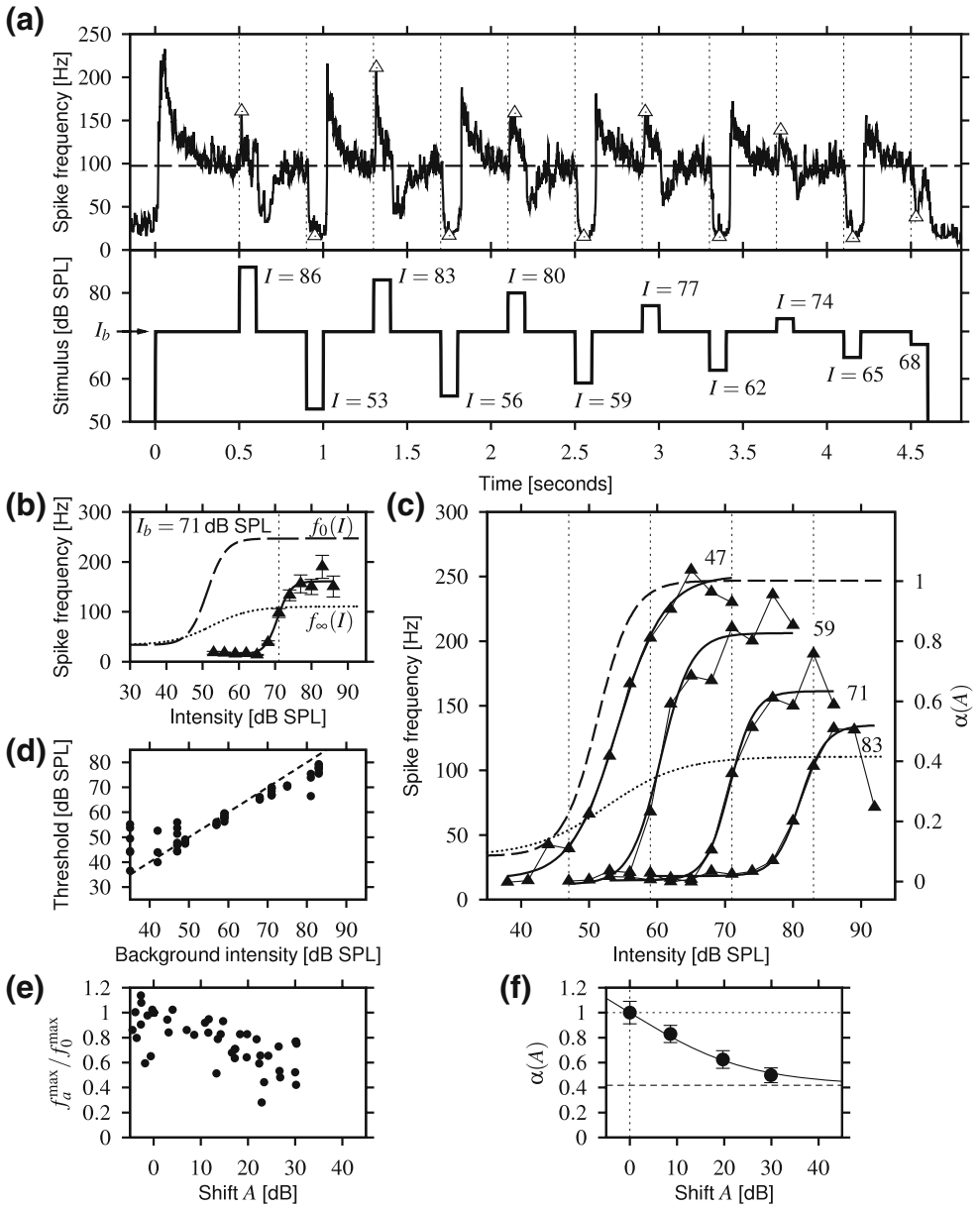

Fig. 7 Adapted f-I curves. (**a**) The stimulus we used for measuring adapted f-I curves is displayed in the *lower panel*. It adapts the cell to a given background intensity I_b (*arrow*) and then tests the response of the cell to different intensities I by short test pulses (100 ms) that are separated by 300 ms. From the spike-frequency response (*solid line*, *upper panel*) we extracted the onset response to the test pulses (*triangles*). The *dashed line* is the averaged spike frequency just before the test pulses, the *vertical lines* indicate the onset of the test pulses. (**b**) The adapted f-I curve (*triangles* with standard error) that we obtained from the measurement shown in (**a**). The *solid line* is a Boltzmann function (1) that we fitted to the data. The fits to the onset (*dashed line*) and the steady-state f-I curves (*dotted line*) from Fig. 6(a) are shown for comparison. The *vertical line* indicates the background intensity to which the cell was adapted. (**c**) All adapted f-I curves measured in a single cell. The f-I curves are labeled with the corresponding background intensity in dB SPL. In addition, the background intensities are indicated by the *vertical lines*. (**d**) The thresholds of all adapted f-I curves measured as a function of the background intensity I_b. The *dashed line* is the identity. (**e**) The dependence of the relative maximum spike frequency of all adapted f-I curves on the shift A of their threshold relative to the respective onset f-I curve. (**f**) Dependence of the relative maximum spike frequency $\alpha(A) = (f_a^{\max} - f_a^{\min})/(f_0^{\max} - f_0^{\min})$ of the adapted f-I curves shown in (**c**) on their position A relative to the onset f-I curve (c.f. axis labeled $\alpha(A)$ in (**c**)). The *solid line* is a fit of Eq. (8) on the data. The *lower horizontal line* is the relative maximum spike frequency of the steady-state f-I curve (r in Eq. (8))

The function (8) equals one at $A = 0$, decreases linearly with a slope determined by the only free parameter γ, and then exponentially levels out at r (see Fig. 7(f)). A fit of the function (8) to the data yielded on average $\gamma = (0.06 \pm 0.05)\,\mathrm{dB}^{-1}$ and a good description of the data (χ^2-test, $p = 0.999 \pm 0.003$).

3.6 Time constants of adaptation

In this section we investigate how the adaptation strength evolves with time. The present description of the adapted f-I curves is static and does not characterize any dynamics for the adaptation strength. The exponential decay of the spike-frequency response evoked by the constant amplitude stimuli (Fig. 5) suggested a single first order dynamics. In the following we determine the corresponding time constants of adaptation from responses evoked by the same constant amplitude stimuli used for constructing the onset and steady-state f-I curves.

By fitting a single exponential function (5) to the spike-frequency response we obtained the effective time constant of adaptation for different intensities (Fig. 8(a)). In Fig. 8(b) the effective time constants of adaptation from all cells are summarized. For stimulus intensities more than 10 dB above threshold the time constants did not depend on intensity and averaged to $\tau_{\mathrm{eff}} = 62 \pm 14\,\mathrm{ms}$ ($n = 440$). Closer to the threshold it was more difficult to obtain a reliable estimate for the time constants (compare with Fig. 5(c) and the error bars in Fig. 8(a)).

We summarize our findings on spike-frequency adaptation in a phenomenological model (9) below. Briefly, the model describes how the neuron's f-I curve is changed by adaptation. The corresponding dynamics is determined by the adaptation time-constant. We obtained this time constant by fitting the model (9) to the spike-frequency response (gray lines in Fig. 5). Since the onset, adapted, and steady-state f-I curves parameterized by Boltzmann functions (1) were already determined, the adaptation time-constant and the unknown delay between the response and the stimulus were the only two free parameters. The resulting time constants are displayed in Fig. 8(c) for an individual cell and in Fig. 8(d) for all cells. There was no significant dependence for the adaptation time-constant on

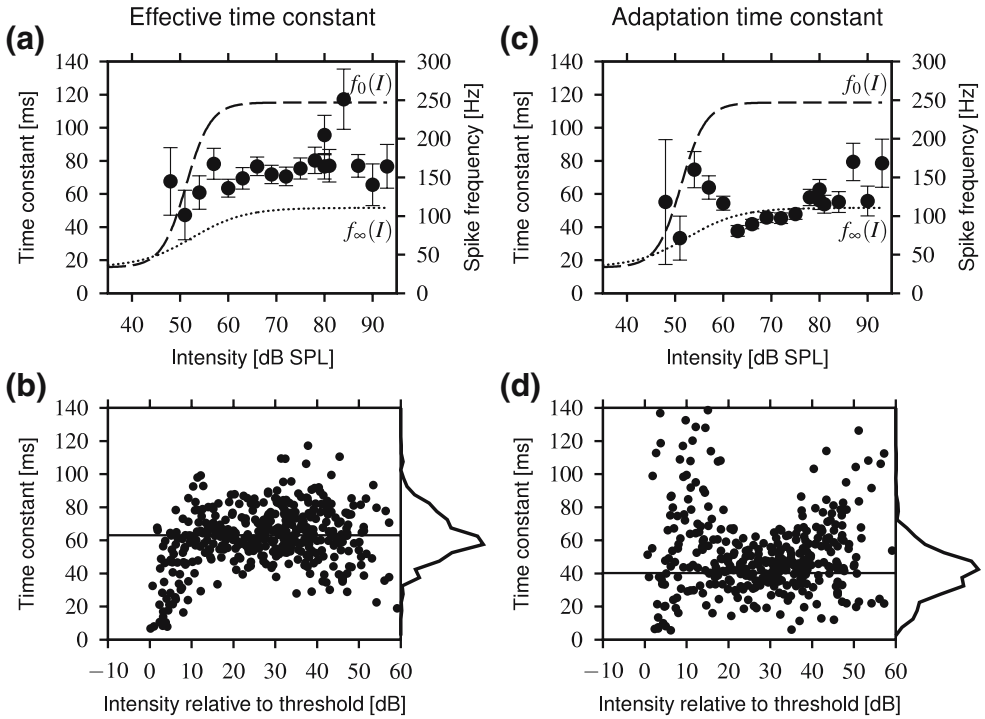

Fig. 8 Time constants of adaptation. (**a**) Effective time constants of adaptation (*left axis*) of a single cell that we obtained by fitting a single exponential (5) on the response to constant amplitude stimuli presented at different intensities (*dashed lines* in Fig. 5) in comparison with the onset (*dashed line*) and steady-state $f - I$ curve (*dotted line*, *right axis*). (**b**) The effective time constants from all cells as a function of stimulus intensity relative to the threshold of the onset f-I curve. The *solid line* is the average (62 ms) of all time constants more than 10 dB above threshold and the corresponding histogram is shown to the *right*. (**c**) The adaptation time-constants of the same cell as in (**a**) that was obtained by fitting the spike frequency computed by the model (9) to the response to constant amplitude stimuli (*gray lines* in Fig. 5). (**d**) Adaptation time-constants from all cells. The average of all adaptation time-constants 20 dB above threshold is 40 ms (*solid line*; histogram shown to the *right*)

stimulus intensity for the ranges below or above 20 dB relative to threshold. The average of all time constants measured at more than 20 dB above threshold was $\tau = 41 \pm 16$ ms ($n = 312$). The adaptation time-constant derived from the model differs from the effective time constant (Fig. 8(b,d)) for two reasons. Firstly, because the time course of the adaptation strength A, which is governed by τ, is mapped through the nonlinear shape of the adapted f-I curve, and secondly, since the maximum spike frequency of the adapted f-I curve depends additionally on A.

3.7 A phenomenological model for the AN1's spike-frequency response

Based on the data on spike-frequency adaptation we are able to construct a phenomenological model for the dynamics of the spike-frequency response of the AN1 following the framework introduced by Benda and Herz (2003). The model allows to predict the response of the AN1 to time varying stimuli and to assess the role of adaptation in creating the observed intensity invariance Fig. 2.

Assuming that adaptation evolves on a timescale much slower than the spike generating processes allows for a separation of the two dynamics. Typical interspike intervals in the AN1 response are less than 10 ms long and shorter than the timescale of spike-frequency adaptation (40 ms, Fig. 5(a)), thus justifying this assumption. Since we are primarily interested in the spike-frequency response over time and not in the timing of the spikes, the dynamics of the spike generator can be approximated by a direct mapping of the stimulus into a spike frequency through the neuron's f-I curve, provided the stimulus is approximately constant during an interspike interval. Since the spike-frequency response is adapting, the f-I curve is not a fixed function, but dynamically depends on the current strength of adaptation.

The model then has the following structure:

$$f(t) = f_a\big(I(t); A(t)\big) \tag{9a}$$

$$\tau \frac{\mathrm{d}A(t)}{\mathrm{d}t} = A_{\max}(t) - A(t)\ . \tag{9b}$$

The spike-frequency response $f(t)$ at time t is given by the stimulus $I(t)$ that is mapped through the adapted f-I curve $f_a(I; A)$ (Eq. (11) or (12) below). We assume that the adaptation strength A obeys a linear first order dynamics (9b), where A approaches a steady-state $A_{\max}$ with the adaptation time-constant τ. The time dependence of $A_{\max}(t)$ follows from its dependence on the stimulus $I(t)$ (see Eq. (13) below). Note also that there is a unknown delay due to axonal delays and synaptic transmission between the stimulus and the response that has to be taken into account when comparing the model prediction with measured data.

The response of the unadapted neuron, where the adaptation strength equals zero, is given by the onset f-I curve

$$f_a(I; A = 0) \equiv f_0(I) \tag{10}$$

that we parameterize with a Boltzmann function (1).

From the measurements of adapted f-I curves we gain the necessary information about their dependence on A. We have shown above (Fig. 7) that the adapted f-I curves are shifted to higher intensities. If we identify the adaptation strength A with the shift of the adapted f-I curves (threshold of the adapted f-I curve minus threshold of the onset f-I curve), then the adapted f-I curve is simply the onset f-I curve shifted by A to higher stimulus intensities:

$$f_a(I; A) = f_0(I - A)\ . \tag{11}$$

This shift, however, is accompanied with a reduction of the maximum spike frequency. To account for this reduction we multiply the onset f-I curve in Eq. (11) with the factor $\alpha(A) \le 1$ (Eq. (8), Fig. 7(f)) and replace k_0 in the Boltzmann function (1) describing $f_0(I)$ by $k_0/\alpha(A)$ in order to keep the slope of the f-I curves the same. In addition, we want the threshold of the Boltzmann function to be unaffected by the scaling with $\alpha(A)$. Therefore, the position parameter I_0^0 in the Boltzmann function needs to be replaced by $I_0^0 - \frac{2}{k_0}\big(1 - \alpha(A)\big)$. In summary, we get the following functional form for the adapted f-I curves

$$f_a(I; A) = \frac{\alpha(A)(f_0^{\max} - f_0^{\min})}{1 + \exp\left(-\frac{k_0}{\alpha(A)}\left(I - I_0^0 + \frac{2}{k_0}(1 - \alpha(A)) - A\right)\right)} + f_0^{\min}\ . \tag{12}$$

Graphs of this function are displayed in Fig. 7(c) for a particular cell.

The distance between the onset and the steady-state f-I curve determines $A_{\max}$ in Eq. (9b). Assuming that

the adaptation process is mainly driven by the input identifies $A_{\max}$ as

$$A_{\max} = I - f_0^{-1}\left(f_\infty(I)\right) , \tag{13}$$

where $f_0^{-1}(f)$ is the inverse onset f-I curve.

For stimuli fluctuating faster than the width of an interspike interval it is necessary to specify dynamics for the generation of spikes in addition to the adaptation dynamics. The simplest extension that does not require any additional parameter is to reinterpret the spike frequency $f(t)$ as computed by the adaptation model (9) as a phase velocity and to feed it into a perfect integrator

$$\frac{\mathrm{d}\varphi}{\mathrm{d}t} = f(t) \tag{14}$$

that integrates the phase variable φ. Whenever φ reaches one a spike is emitted and φ is reset to zero.

Equation (14) can be interpreted in a continuous way as well. For each point in time, $f(t)$ is integrated symmetrically backward and forward in time until the integral equals one. Then the spike frequency at t is the inverse width of the integration interval. This corresponds to a sliding average with the width of the averaging window given by the resulting spike frequency. In the following we denote this smoothing operation on the spike frequency from Eq. (9a) by angled brackets $\langle f(\cdot)\rangle$.

The resulting prediction of the spike-frequency can then be compared with the measured response evoked by the same stimulus. Further, the model allows to directly compute the transfer function of an adapting neuron once the required parameters (f-I curves and adaptation time constant) are determined from the experiments with constant stimuli.

3.8 Predicting the spike-frequency response to RAM stimuli

Knowing the onset, adapted, and steady-state f-I curves and the adaptation time-constant of a specific neuron from the experiments with constant amplitude stimuli completely defines the adaptation model (9). We then were able to predict the spike-frequency response of each cell to various other stimuli. In Fig. 9 two examples with RAM stimuli are shown and in Table 2 the performance of several variants of the model is summarized.

Simply mapping the stimulus through the onset or steady-state f-I curve, thus neglecting any adaptation dynamics, obviously did not reproduce the measured spike-frequency response(Fig. 9(a-2)). The spike-frequency obtained from the onset f-I curve drastically overestimated the response. The mean difference between the predicted and the measured spike frequency was 99 ± 25 Hz (in total $n = 240$ stimuli measured in 13 cells). For the steady-state f-I curve the mean difference was close to zero (-3 ± 8 Hz). However, the correlation between predicted and measured spike frequency was poor for both scenarios ($r = 0.3 \pm 0.1$), indicating that some features of the measured spike frequency were not sufficiently reproduced.

The spike frequency obtained directly from the adaptation model (9) and (12) (dashed lines in Fig. 9(a-3,b-1)) was better correlated with the measured spike frequency ($r = 0.6 \pm 0.2$), but the root-mean-squared (rms) difference between the predicted and measured spike frequency was quite high (37 ± 10 Hz). Whereas the time course of the spike frequency was predicted better for slowly changing stimuli (rms= 31 ± 7 Hz for RAM stimuli with cutoff frequency 50 Hz, $n = 60$, Fig. 9(a-3)), faster changing stimuli resulted in equally fast fluctuating predictions that were not present in the measured response (rms= 41 ± 9 Hz for RAM stimuli with cutoff frequency 400 Hz, $n = 60$). This effect is already visible for RAM stimuli with 100 Hz cutoff frequency as in Fig. 9(b-1). Therefore, the high rms difference of the plain adaptation model might have been due to the missing low-pass filter due to the dynamics of the spike-generator.

Adding a perfect integrator (14) in the interpretation of a smoothing filter to the adaptation model accounted for the basic low-pass filter properties of a spike generator and improved the performance of the adaptation model considerably (gray line in Fig. 9(a-3,b-1)).The mean difference from the measured response of 3 ± 9 Hz was still close to zero, but the rms difference was significantly smaller (22 ± 5 Hz, t-test: $p \ll 0.0001$) and the correlation was significantly stronger ($r = 0.8 \pm 0.1$, t-test: $p \ll 0.0001$). A χ^2-test showed that it is very likely to obtain the observed difference between the measured data and the model prediction (median $p = 1.0$, only 15 from $n = 240$ are below $p = 0.99$).

The absolute values of the rms differences were smaller than the modulation depth (standard deviation)of the spike-frequency response (Fig. 3(b)). On average this prediction error (rms difference of the prediction divided by the modulation depth) was 69 ± 12 % ($n = 240$). For the examples shown in Fig. 9(a-3,b-1) the rms differences were both 23 Hz resulting in prediction errors of 45 and 54%, respectively. The standard deviation associated with the spike frequency (inter-trial variability) was 56 Hz (averaged over the whole stimulus duration and all 240 stimulus presentations)—about twice the averaged rms differences. However,

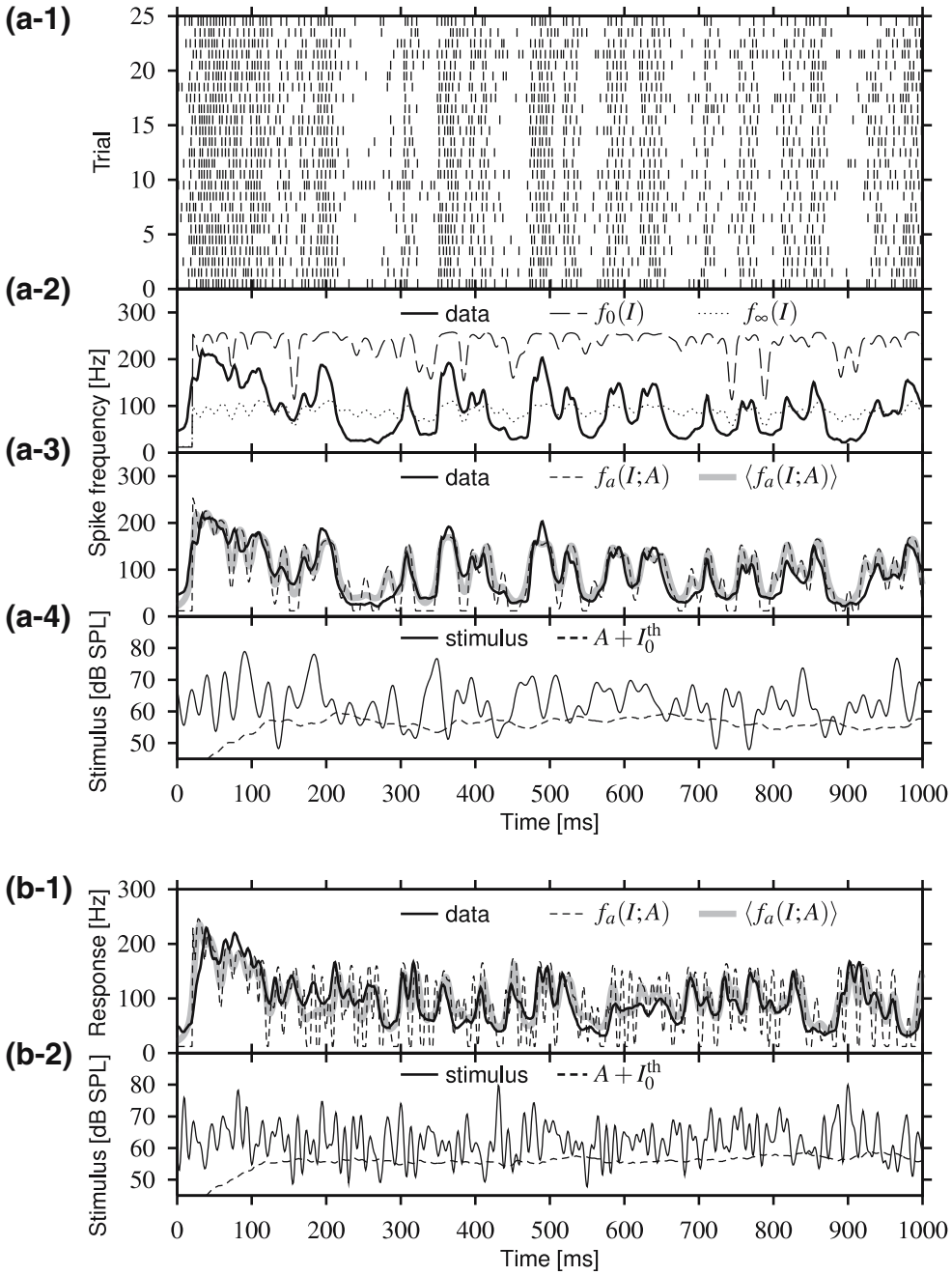

Fig. 9 Model performance for RAM stimuli. (**a-1**) The spike trains evoked by repeated presentation of the RAM stimulus shown in (**a-4**). (**a-2**) The spike-frequency response (*solid line*) computed from the spike trains shown in (**a**) in comparison with the spike frequency that one would expect by simply mapping the stimulus through the onset f-I curve (*dashed line*) or the steady-state f-I curve (*dotted line*). Neither matches the observed response. **(a-3)** The spike-frequency response predicted by the adaptation model alone (Eqs. (9) and (12), *dashed line*) and in combination with the perfect integrator (14) to approximate the dynamics of the spike-generator (*thick gray line*). Both describe the measured response (*solid line*) well. (**a-4**) The stimulus (*solid line*) was a RAM with cutoff frequency 50 Hz, standard deviation 6 dB and mean intensity 62 dB SPL. The *dashed line* displays the threshold of the adapted f-I curve, which shows the dynamics of the adaptation strength A computed by the model (9b) added to the threshold of the onset f-I curve. Only stimulus components above this line result in responses. Note, however, that there is a delay between $A(t)$ and the spike frequency response on one hand and the stimulus on the other hand. (**b-1**) Since the plain adaptation model (9) directly maps the stimulus through an f-I curve, the predicted spike-frequency response (*dashed line*) follows arbitrarily fast fluctuations of the stimulus that are not visible in the measured spike frequency (*solid line*). Combining the adaptation model with the perfect integrator (14) and thus accounting for the low-pass filter introduced by the dynamics of the spike-generator results in a better prediction (*thick gray line*) of the measured data. (**b-2**) The stimulus was a RAM with cutoff frequency 100 Hz, standard deviation 6 dB and mean intensity 62 dB SPL

Table 2 Performance of the models

Model	Mean difference [Hz]	Rms diff. [Hz]	Correlation
Without adaptation:			
Onset f-I curve $f_0(I)$	105 (86–116)	110 (96–122)	0.29 (0.24–0.33)
Steady-state f-I curve $f_\infty(I)$	−2.7 (−8.5–1.9)	31 (26–36)	0.31 (0.25–0.40)
Adaptation with reduction of maximum spike frequency, Eqs. (9) and (12):			
Adaptation only $f_a(I; A)$	1.0 (−5.1–7.4)	35 (30–44)	0.58 (0.47–0.72)
Adaptation plus integrator $\langle f_a(I; A)\rangle$	3.6 (−3.0–9.9)	21 (18–24)	0.82 (0.76–0.86)
Adaptation with shift only, Eqs. (9) and (11):			
Adaptation plus integrator $\langle f_0(I - A)\rangle$	12 (6.9–18)	24 (20–29)	0.83 (0.78–0.86)

The table summarizes the medians (with 1. and 3. quartile in brackets, $n = 240$) of the mean difference, the rms difference, and the correlation between the predicted and measured spike-frequency responses to RAM stimuli (50, 100, 200, 400 Hz, 4 and 6 dB, mean intensities 52, 62, 72 dB SPL)

keep in mind, that with a single set of parameters for each cell (the parameterization of the onset, adapted, and steady-state f-I curves and the adaptation time constant) the model predicted the spike-frequency response to a whole range of different stimuli with different mean intensities with similar accuracy (see also Fig. 10). It might therefore be more appropriate to compare the rms-difference values with the whole range of possible spike-frequencies, which is about 200 Hz—about ten times the averaged rms differences.

In Fig. 10 the prediction of the adaptation model (9) and (12) with perfect integrator (14) (gray lines) for a RAM stimulus with 50 Hz cutoff frequency and 6 dB standard deviation presented at three different mean intensities is compared with the measured spike frequency (black lines). In this example the responses to all three intensities were reproduced equally well by the model.

The model performance pooled over all cells and all RAM stimuli as a function of the mean intensity of the stimuli is displayed in Fig. 10(d). All three measures (mean difference, rms difference, and correlation between measured and predicted spike frequency) showed only small differences between the intensities. Thus, the model successfully predicted the spike-frequency response to all RAM stimuli irrespective of their mean intensity. This demonstrates that the adaptation dynamics is indeed sufficient to explain the observed intensity invariance.

3.9 Role of the reduction of the maximum spike frequency

In order to asses the impact of the reduction of the maximum spike frequency that we observed for the adapted f-I curve (Fig. 7) we also analyzed the performance of a simpler adaptation model that does not incorporate this reduction but only shifts the onset f-I curve to higher intensities (Eqs. (9) and (11), last row in Table 2). This model overestimated the measured spike frequency in response to the RAM stimuli by 12 ± 9 Hz and the rms difference was significantly higher (25 ± 7 Hz, t-test: $p \ll 0.0001$) than the one of the adaptation model including the reduction of the maximum spike frequency (Eqs. (9) and (12)). These differences, however, were small and demonstrate that the reduction of the maximum spike frequency did not play a major role in shaping the response to the RAM stimuli.

In Fig. 11 we compare the predictions of the two models for the spike-frequency response evoked by pulse AM stimuli resembling cricket songs. In this example there is a difference in the model predictions during the pulses visible (Fig. 11(a-2,b-1)). The model not including the reduction of the maximum spike frequency (dashed line) overestimated the measured response. This observation was verified by the statistics of the model performance evaluated between 200 and 500 ms after stimulus onset pooled over all 13 cells ($n = 100$). The mean difference (with reduction: 5 Hz (−2–13 Hz), without reduction: 31 Hz (25–39 Hz), median with 1. and 3. quartile in brackets) as well as the rms difference (with reduction: 20 Hz (15–26 Hz), without reduction 42 Hz (37–48 Hz)) between the prediction and the measured response were both significantly larger (t-test: $p \ll 0.0001$) in the model not including the reduction of the maximum spike frequency. Thus, in response to the pulse AM stimuli the reduction of the maximum spike frequency does play a role.

Furthermore, during the first pause of a pulse AM stimulus the cells showed some spiking activity although there wasn't any stimulus (arrow in Fig. 11a-2). Consequently, the model (9), (12), and (14) underestimated the initial response to all pulse AM stimuli by −13 Hz (−19–0 Hz) (mean difference between predicted and measured response, median with

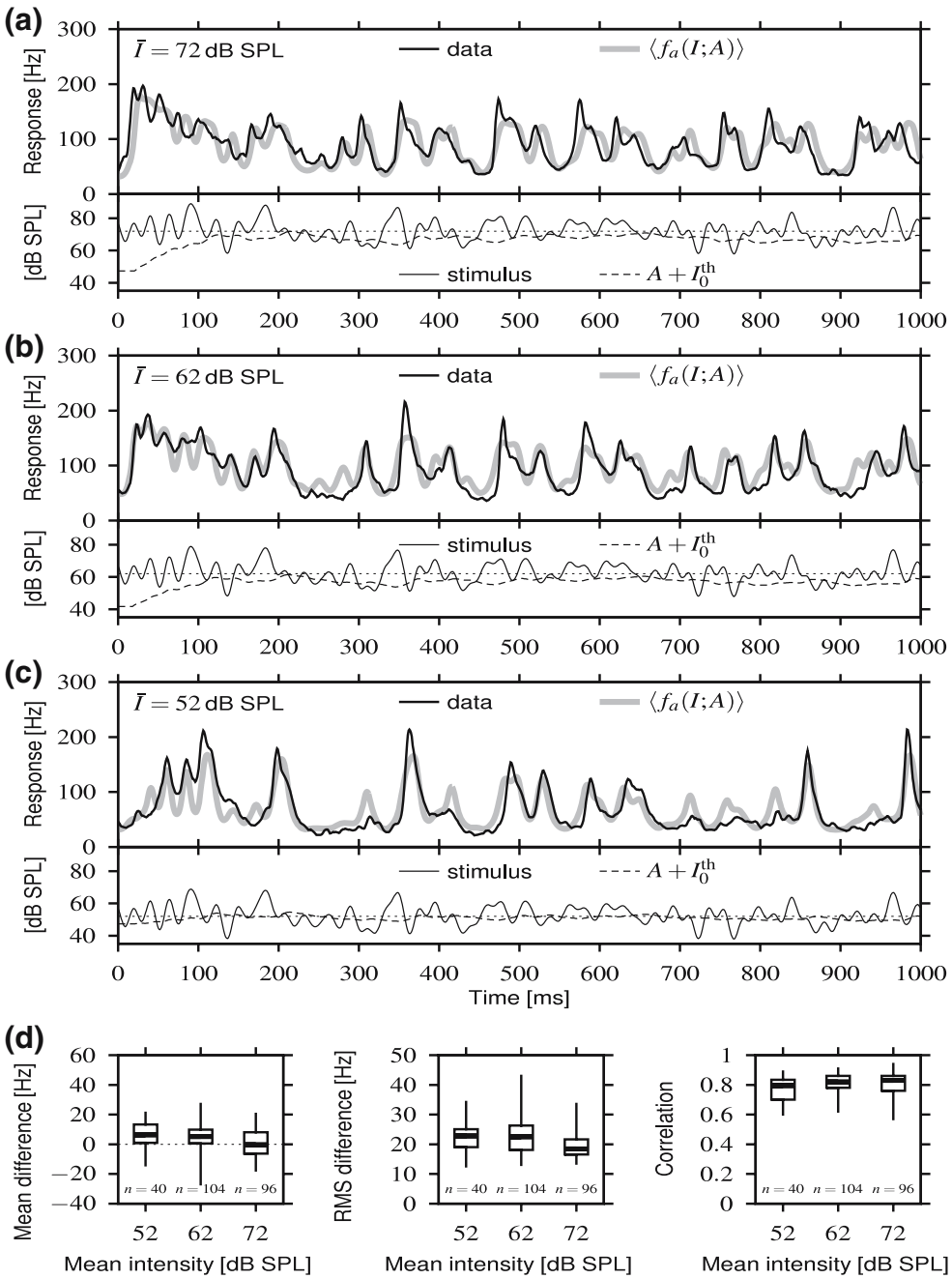

Fig. 10 Model performance and intensity invariance. (**a–c**) The spike-frequency responses (*black line*, *upper panels*) evoked by RAM stimuli with cutoff frequency 50 Hz and standard deviation 6 dB (*lower panels*, *solid line*) presented at three different mean intensities $\bar{I} = 72$, 62, 52 dB SPL as indicated. The *gray line* in the *upper panels* is the prediction of the adaptation model (9) and (12) in combination with the perfect integrator (14). The *dashed line* in the *lower panels* displays the time course of the threshold of the adapted f-I curve, which is the threshold of the onset f-I curve I_0^{th} plus the time course of the adaptation strength A as computed by the adaptation model (9b). (**d**) The mean difference, the rms difference, and the correlation between the predicted and measured spike frequency computed during one second of stimulation with the RAM stimuli (cutoff frequencies 50, 100, 200, or 400 Hz, standard deviations 4 or 6 dB, mean intensities 52, 62, or 72 dB SPL) summarized from all 13 cells. Values are medians (*thick line*) with 1. and 3. quartile (*box*) and minimum and maximum value (*whiskers*)

1. and 3. quartile) within 0 and 200 ms after stimulus onset (see Section 4).

3.10 Transfer function and intensity invariance

The adaptation model (9) allows us to assess the signal transmission properties of the AN1 for time varying stimuli solely from the measured f-I curves and the adaptation time-constant that we determined using constant stimuli.

Low-frequency components of a stimulus are attenuated by adaptation and are mapped through the steady-state f-I curve. On the other hand, high-frequency components are transmitted through the adapted f-I curves which are steeper than the steady-state f-I curve (Benda and Herz 2003). Therefore, spike-frequency adaptation turns a neuron into a high-pass filter (Nelson et al. 1997; French et al. 2001; Benda and Herz 2003; Benda et al. 2005). Since the steady-state f-I curve of the AN1 is approximately independent of the stimulus intensity for intensities above

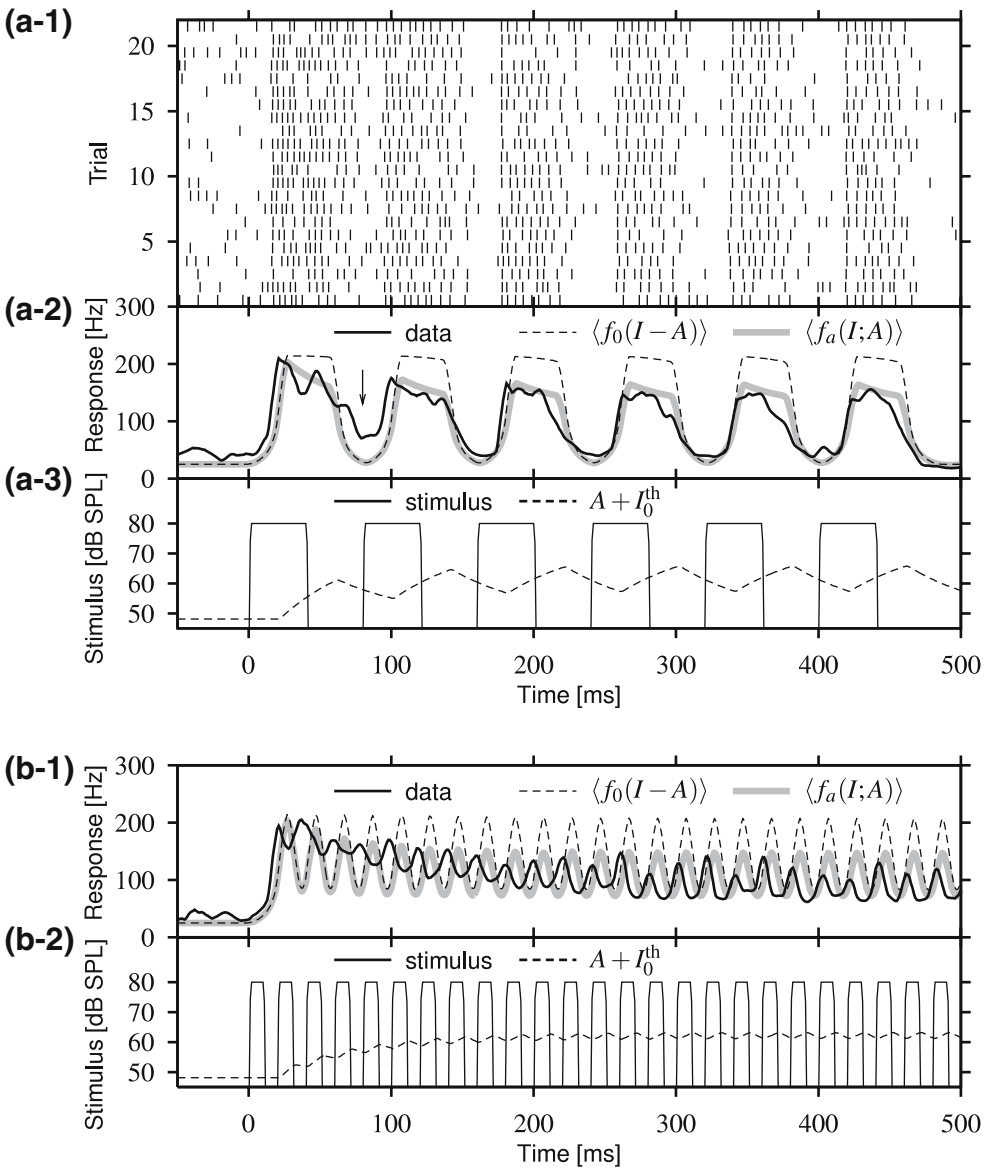

Fig. 11 Model performance for a pulse stimulus. (**a-1**) The spike trains evoked by repeated stimulation with the pulse AMs shown in (**a-3**). (**a-2**) The spike-frequency obtained from the spike trains (*solid line*) in comparison with predictions from the adaptation model (9) and (14) with shifted f-I curve ((11), *dashed line*) or including the reduction of the maximum spike-frequency ((12), *thick gray line*). The *arrow* indicates a unexpected high measured response during the first pause of the stimulus. (**a-3**) The pulse AM stimulus was presented at 80 dB SPL. Pulses and pauses were each of 40 ms duration. The *dashed line* displays the threshold of the onset f-I curve I_0^{th} plus the time course of the adaptation strength A as computed by the adaptation model (9b) and (12). (**b**) Responses to a pulse AM stimulus with pulses and pauses each of 10 ms duration at 80 dB SPL. Note the low modulation of the spike-frequency response during the first pulses

about 60 dB SPL (Fig. 6(a)), slow stimulus components change the output spike-frequency only marginally, and hence the response is intensity invariant.

The detailed signal transmission properties of a linear system can be characterized by its transfer function, which describes the gain and phase shift of the output for each frequency component of the stimulus. The saturation level of the steady-state f-I curve of the AN1 at about 100 Hz sets a spike frequency around which the dynamics of the adaptation model can be linearized as illustrated in Fig. 12(a) and described in the Appendix. The gain (22) of the resulting transfer function as a function of stimulus frequency resembles a high-pass filter and is shown in Fig. 12(b) (solid line). The gain approaches its maximum value, which equals the slope of the onset f-I curve, at frequencies above a cutoff frequency $f_{\text{cutoff}} = (2\pi\tau)^{-1} = 4.0 \pm 1.4$ Hz, that is determined by the adaptation time-constant τ (Fig. 8(d)). For low stimulus frequencies below the cutoff frequency the gain decreases down to zero, i.e. slow stimulus components including the stimulus' mean intensity are filtered out. Thus the filter properties derived from the adaptation properties of the AN1 sufficiently account for the observed intensity invariance.

The spike-generator itself acts like a low-pass filter whose cutoff frequency depends approximately linearly on the spike frequency ν (Fourcaud-Trocmé et al.

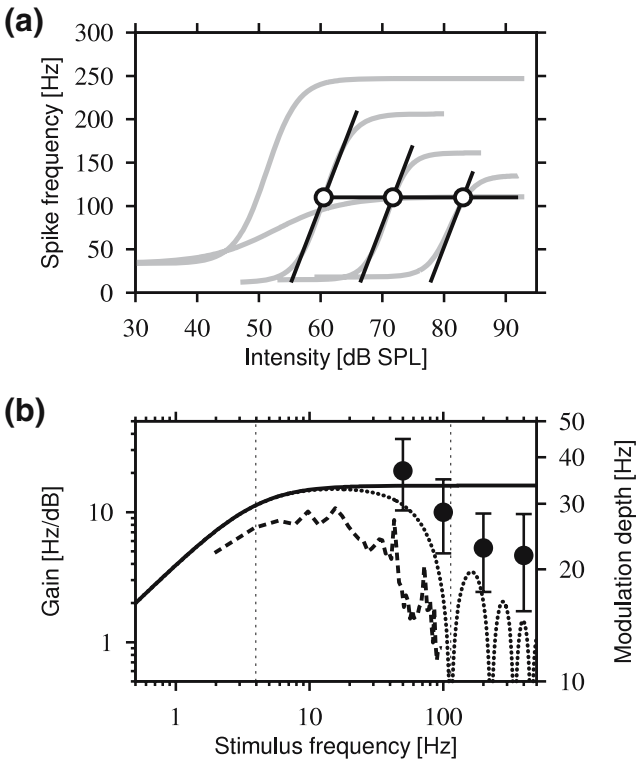

Fig. 12 Transfer function of the linearized adaptation model for the AN1. (**a**) Linearization of the adaptation model. The experimentally measured onset, steady-state, and adapted f-I curves from Fig. 7(c) are plotted in *gray*. The *solid lines* are linearizations of the steady-state f-I curve (16) (with $s_\infty = 0$, and $\hat{f}_\infty = f_\infty^{\max}$) and the adapted f-I curves (18) around the maximum steady-state spike frequency at 100 Hz (*circles*). (**b**) The gain (*dotted line*) of the AN1 as a function of the stimulus frequency is composed of the high-pass filter due to adaptation (*solid line*) and the low-pass filter of the spike generator. The gain is computed using Eqs. (22) and (15), the averaged slope of the AN1's onset f-I curve of 16 Hz/dB, adaptation time constant of 40 ms, and steady-state firing rate of 114 Hz (see Table 1). The *vertical lines* mark the cutoff frequency of the high-pass filter (4 Hz) and the averaged spike frequency that determines the low-pass filter (114 Hz). For comparison, the average gain computed from all responses to the RAM stimuli with cutoff frequency 100 Hz and mean intensities 62 and 72 dB SPL is plotted (dashed line). The modulation depth of the experimentally measured responses evoked by RAM stimuli as a function of their cutoff frequency (*filled circles*, mean with standard deviation) also follows the 114 Hz low pass filter

(2003). For the perfect integrator (14) the transfer function reads

$$H_s(\omega) = \frac{\sin(\omega v/2)}{\omega v/2} \tag{15}$$

(Knight 1972). Intuitively, the time course of a stimulus can be easily inferred from the spike frequency provided there are several spikes per stimulus fluctuation. On the other hand, from a single interspike interval it is difficult to infer whether it was generated by a stimulus that was approximately constant during the interspike interval or fluctuating once or several times. Thus, using a low-pass filter with a fixed cutoff frequency would in general not capture this fundamental property of neuronal filtering. However, since the steady-state f-I curve of the AN1 saturates at about 100 Hz, the experimentally measured mean spike-frequency evoked by various stimuli is about 100 Hz for mean stimulus intensities above about 60 dB SPL (see Fig. 3(a)). Therefore, for the AN1 the cutoff frequency of the corresponding low-pass filter is to a first approximation independent of the mean stimulus intensity. The combined transfer function (Fig. 12(b), dotted line) is therefore independent of the mean stimulus intensity as well.

From the spike-frequency responses to the RAM stimuli the gain can be directly computed (Fig. 12(c), dashed line). Both the predicted high-pass filter due to adaptation and the low-pass filter due to the spike generator are verified by the data. Note, that since the spike-frequency is not fixed at 100 Hz the singularities of the lowpass filter (15) at multiples of the cutoff frequency are smeared out and therefore not visible in the real data.

As an indirect indicator for the low-pass filter effect of the spike generator we plotted the modulation depth of the experimentally measured spike-frequency response evoked by the RAM stimuli as a function of their cutoff frequency in Fig. 12(c) (filled circles). The modulation depths follow the overall decay of the gain function, thus confirming the existence of a low-pass filter with a cutoff frequency at about 100 Hz.

4 Discussion

We demonstrated that intensity invariance as a first step towards feature extraction in crickets is already implemented at the level of first order neurons in auditory processing (Figs. 2, 3 and 4). Spike-frequency adaptation operating on a short timescale of 40 ms (Figs. 5 and 8) fully accounts for the dynamics of this intensity invariance, as we have shown by means of the phenomenological model, Eqs. (9), (12), and (14), which is the simplest possible description of the data we obtained from characterizing adaptation with constant amplitude stimuli (Figs. 5, 6 and 7). Using the model we successfully predicted the response to dynamic stimuli (Figs. 9, 10 and 11) and determined the transfer function of the AN1-neuron (Fig. 12).

4.1 Spike-frequency adaptation and intensity invariance

Based on the good performance of the phenomenological adaptation model, Eqs. (9), (12) and (14), we

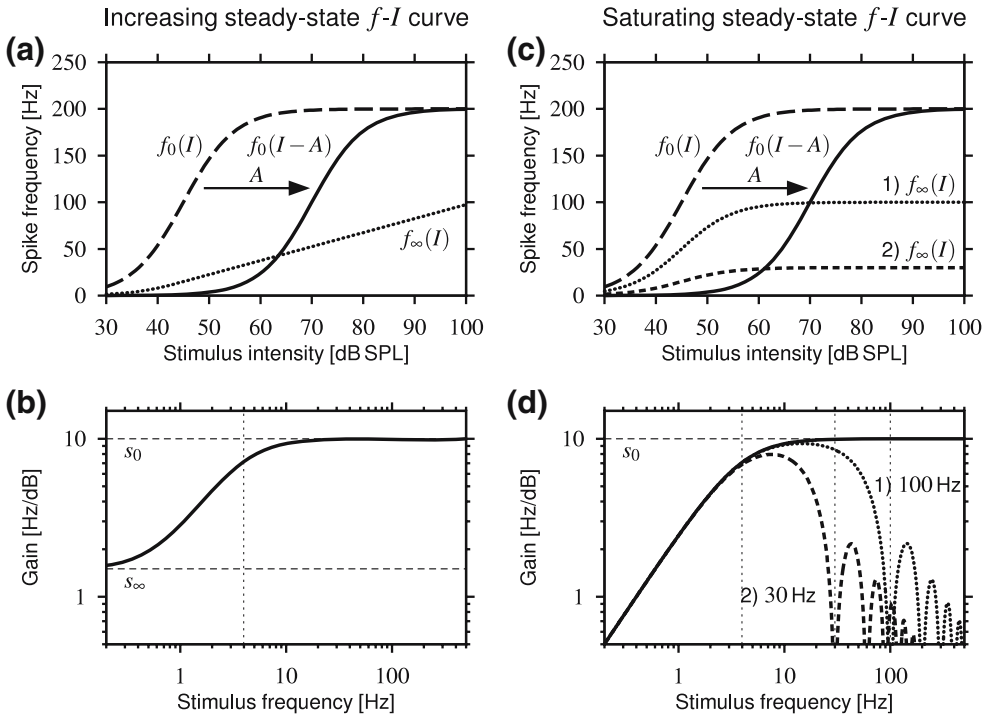

Fig. 13 Gain of adapting neurons. (**a**) Onset f-I curve ($f_0(I)$, *dashed line*) and steady-state f-I curve ($f_\infty(I)$, *dotted line*) of a hypothetical neuron. Here, the steady-state f-I curve is increasing approximately linearly with stimulus intensity (slope is 1.5 Hz/dB). The main effect of spike-frequency adaptation is a subtractive reduction of the stimulus intensity by the strength of adaptation A that results in a shift (*arrow*) of the onset f-I curve to higher stimulus intensities (*solid line*). (**b**) The transfer function for the spike-frequency response of an adapting neuron (20) is a high-pass filter. Plotted is the gain ((21), *solid line*) calculated for the linearized adaptation model (19). Stimulus components faster than the cutoff frequency (*vertical line*) of the filter are transmitted with a gain set by the slope s_0 of the onset f-I curve, slower stimuli with a gain set by the slope s_∞ of the steady-state f-I curve. (**c**) In contrast to the scenario described in (**a**) and (**b**) we consider here two scenarios where the steady-state f-I curve saturates at a spike frequency of 1) 100 Hz (*dotted line*) or 2) 30 Hz (*short dashed line*). (**d**) For stimuli with mean intensities in the range where the steady-state f-I curves are approximately flat, the gain ((22), *solid line*) of the adaptation transfer function vanishes for low frequency components. The additional low-pass filter effect due to the spike generator as approximated by Eq. (15) turns the neuron into a band-pass filter (*dotted and dashed lines*). Note that the different steady-state spike frequencies of the two scenarios only influence the low-pass filter component, not the high-pass filter. The *vertical lines* mark the cutoff frequency of the high-pass filter at 4 Hz and the averaged spike frequency that mainly determines the low-pass filter (100 and 30 Hz for scenario (1) and (2), respectively)

conclude that the properties of the observed spike-frequency adaptation are sufficient to describe the dynamics of intensity invariance. Intensity invariance is tightly connected with the high-pass filter properties of adapting neurons (Nelson et al. 1997; French et al. 2001; Benda and Herz 2003; Benda et al. 2005). In particular, it is the shift of the adapted f-I curves along the intensity axis that is necessary for generating the observed intensity invariance, since by shifting the f-I curve low frequency components of the stimulus are filtered out. At the same time the slope of the adapted f-I curve and thus the gain for fast stimulus components is not changed. On the other hand, contrast-invariance requires a divisive effect of adaptation on the adapted f-I curves (Brenner et al. 2000; Fairhall et al. 2001; Reinagel 2001; Maravall et al. 2007). However, we have observed neither divisiveness in the adapted f-I curves (Fig. 7) nor contrast invariance of the AN1's response to RAM stimuli with different standard deviations (Fig. 4).

It is important to note, that spike-frequency adaptation alone is not sufficient to generate intensity invariance. Following Benda and Herz (2003) and Benda et al. (2005), and as demonstrated in Fig. 13(a,b), the steady-state f-I curve transmits low-frequency components of the stimulus with a gain set by its slope (see Appendix for a mathematical derivation of the transfer function). Consequently, for mean stimulus intensities where the steady-state f-I curve has a non-vanishing slope (Fig. 13(a)) the response of the neuron is not invariant with respect to the mean intensity of the stimuli. Intensity invariance requires a flat steady-state f-I curve of an adapting neuron as illustrated in Fig. 13(c,d). Studies on adaptation in which the steady-

state f-I curve was not shown to be constant therefore do not allow a conclusive decision about invariant responses of the recorded cells (see for example reports on adaptation in the auditory and visual domain as in Smirnakis et al. 1997; Sanchez-Vives et al. 2000; Kim and Rieke 2003; Kvale and Schreiner 2004; Solomon et al. 2004; Dean et al. 2005).

The high-pass filter properties due to adaptation are independent of the specific spike-frequency where the steady-state f-I curve levels out (Fig. 13(c,d)). The high-pass filter (22) is completely determined by the adaptation time constant and the slope of the onset f-I curve. However, the saturation level of the steady-state f-I curve defines the mean spike frequency of the response to a stimulus and thus largely determines the cutoff frequency of the low-pass filter (15) due to the spike generator.

4.2 Model performance and limitations

The phenomenological model of spike-frequency adaptation we used for our analysis was in its original form derived for adaptation currents of a single neuron (Benda and Herz 2003). It is therefore remarkable that this modified model successfully combines the dynamics of about 50 auditory receptor neurons, their synapses, and of the AN1 itself in its single first-order differential equation. In addition to the original model we included the reduction of the maximum spike frequency of the adapted f-I curve and we assumed a dynamics driven by the stimulus instead of the spike-frequency. Despite the complexity of the involved processes the exponential decay of the spike-frequency in response to constant amplitude stimuli already suggested that a simple dynamic might be sufficient (Fig. 5). The timescale we obtained for the adaptation process (40 ms) was slower than most of the interspike intervals (about 10 ms), thus confirming the necessary separation of the adaptation dynamics from the dynamics of the spike generator (Cartling 1996; Wang 1998; Benda and Herz 2003).

However, the model prediction systematically deviated from the AN1 response during the initial phase of the response to the pulse AM stimuli (Fig. 11(a-2, b-1)). The AN1 kept firing during the pauses of the pulse AM stimulus where there wasn't any stimulus exciting the auditory system. At the high intensities used for the pulse AM stimuli it is possible that few false-positive spikes originating from the onset response of the AN2 caused this phenomenon. During the pulses as well as for the RAM stimuli, however, the model described the adaptation dynamics very well.

4.3 Intensity invariance of the AN1's response

Since the steady-state f-I curve increases approximately linearly with a slope of 3.4 Hz/dB for low stimulus intensities below about 60 dB SPL (Table 1 and Fig. 6(a)) we do not expect intensity invariance for the response of the AN1 in this intensity range. This explains the lower mean firing rate evoked by the low-intensity RAM stimuli as well as the low correlation and slope of the regression line between the responses to low- and high-intensity stimuli (Figs. 2 and 3).

At 60 dB SPL the steady-state f-I curve levels out at a spike frequency of approximately 100 Hz and we therefore expect intensity invariance in the AN1's response for stimuli with mean intensities above this intensity. Indeed the medium- and high-frequency RAM stimuli evoked similar responses in the AN1 (Fig. 3). The adapted f-I curves we measured suggest that this range extends at least up to 85 dB SPL. Ideal intensity invariance would require a pure shift of the adapted f-I curves without a reduction of their maximum spike frequency (as in Fig. 7). However, the observed reduction of the maximum spike frequency of the adapted f-I curves resulted in only a slight decrease in modulation depth of the response to the high-intensity RAM stimuli (Fig. 3(b)) and made only a small difference in predicting the RAM response by the adaptation model (Table 2).

Our analysis focused on the mean spike-frequency response, neglecting other aspects of the AN1's spiking response such as variability, interspike-interval distribution, and correlations. For the AN1 in crickets Marsat and Pollack (2005) observed significant differences in the response-to-response coherence between medium- and high-intensity RAM stimuli (their Fig. 1(a)). For the motion sensitive H1-cell in the fly's visual system, whose response was shown to be invariant with respect to the variance of a motion stimulus, Fairhall et al. (2001) also demonstrated that the interspike-interval distribution contained information about the stimulus variance. It is therefore conceivable that information about the mean stimulus intensity might still be present in the spike trains of the AN1's response, encoded by other means than the average spike frequency.

The timescale on which the AN1 response adapts to changes of the mean intensity of the stimulus is set by the adaptation time-constant (about 40 ms). This time constant determines the cutoff frequency of a high-pass filter at 4 Hz. The dynamics of the spike generator introduces a low-pass filter with a cutoff frequency related to the spike frequency (Knight 1972; Fourcaud-Trocmé et al. 2003). The reduction of the spike frequency by

adaptation therefore reduces the temporal resolution of the response. However, the relatively high saturation level of the steady-state response at about 100 Hz in the AN1 ensures signal transmission with sufficient temporal resolution. The resulting band-pass filter from 4 to 100 Hz (Fig. 12(b)) encompasses the behaviorally relevant range of communication signals in crickets (Doolan and Pollack 1985; Schildberger 1984; Huber et al. 1989; Hennig 2003).

The time-constant of the adaptation process we investigated here is much faster than the probably calcium dependent adaptation over several seconds of the Omega neuron known from crickets and bush-crickets (Pollack 1988; Sobel and Tank 1994; Römer and Krusch 2000). This suggests that the auditory system of crickets operates on several timescales as has been reported for several other sensory systems (French and Torkkeli 1994; Xu et al. 1996; Nelson et al. 1997; Baccus and Meister 2002; Nelken et al. 2003; Ulanovsky et al. 2004).

Schildberger (1984) reported that neurons from the song-recognition network in the cricket's brain show intensity invariance above intensity levels of 60 dB SPL. Remarkably, our study demonstrates that this intensity invariance is already generated at the first level of auditory processing. The most likely explanation for the failure to detect this phenomenon earlier is the common method of constructing intensity-response curves from spike counts per entire stimulus (e.g. Schildberger and Hörner 1988; Horseman and Huber 1994b).

Neurons in the auditory midbrain of the guinea pig were shown to adjust their responses to the mean, variance, and more complicated statistics of sound level distributions (Dean et al. 2005). Some of the reported f-I curves share many features, like width of dynamic range, shift of f-I curves, reduction of maximum spike frequency, with the adapted f-I curves that we obtained for the cricket's AN1. However, the adaption timescale of 40 ms we measured in the cricket is much shorter than the timescale of about 3 s Dean et al. (2005) obtained for the adaptation processes in the guinea pig. For the auditory system of crickets, we were able to demonstrate, using instantaneous spike frequency as a measure for the neuron's response and separating onset and steady-state responses, that fast spike-frequency adaptation indeed results in intensity invariance already at the level of the first synapse.

Acknowledgements We thank Laurenz Wiskott and Oliver Behrend for lively discussions and Bernhard Ronacher for critically commenting on the manuscript. Partially funded by DFG, SFB 618 B6.

Appendix

Transfer function of an adapting neuron

Following Benda and Herz (2003) we linearize the f-I curves around a given steady-state spike frequency $\hat{f}_\infty$. We then get for the steady-state f-I curve

$$f_\infty(I) \approx \hat{f}_\infty + s_\infty(I - \hat{I}_\infty) \,, \tag{16}$$

the onset f-I curve

$$f_0(I) \approx \hat{f}_\infty + s_0(I - \hat{I}_0) \,, \tag{17}$$

and the adapted f-I curves

$$f_a(I; A) \approx \hat{f}_\infty + s_0(I - A - \hat{I}_0) \,, \tag{18}$$

where s_0 and s_∞ are the slopes of the onset and steady-state f-I curves, respectively, evaluated at $\hat{f}_\infty$. $\hat{I}_0$ and $\hat{I}_\infty$ are the intensities where the onset and steady-state f-I curves, respectively, have a spike frequency of $\hat{f}_\infty$.

Using the expressions (16), (17), and (18) for the f-I curves, solving Eq. (9a) for the adaptation strength A and inserting in Eq. (9b) results in a single linear differential equation

$$\tau \frac{\mathrm{d}f}{\mathrm{d}t} = -f + \hat{f}_\infty - s_\infty \hat{I}_\infty + s_\infty I + \tau s_0 \frac{\mathrm{d}I}{\mathrm{d}t} \tag{19}$$

for the output spike frequency $f(t)$. The differential equation is driven by both the stimulus $I(t)$ and its time derivative.

Fourier transforming Eq. (19) and neglecting the constant terms $\hat{f}_\infty - s_\infty \hat{I}_\infty$ yields the transfer function as the Fourier-transformed output $\mathcal{F}[f]$ divided by the Fourier-transformed input $\mathcal{F}[I]$

$$H_a(\omega) = \frac{\mathcal{F}[f]}{\mathcal{F}[I]} = s_0 \frac{\frac{s_\infty}{s_0} + \omega^2\tau^2 + i\omega\tau\left(1 - \frac{s_\infty}{s_0}\right)}{1 + \omega^2\tau^2} \,, \tag{20}$$

where $\omega = 2\pi f_c$ is the angular frequency of the frequency component f_c of the stimulus. The gain is the magnitude of the transfer function

$$g(\omega) = |H_a(\omega)| = s_0 \sqrt{\frac{\frac{s_\infty^2}{s_0^2} + \omega^2\tau^2}{1 + \omega^2\tau^2}} \,. \tag{21}$$

In case of a flat steady-state f-I curve, $s_\infty = 0$, the gain reads

$$g(\omega) = s_0 \frac{\omega\tau}{\sqrt{1 + \omega^2\tau^2}} \,. \tag{22}$$

Note that for slow frequency components ($\omega\tau \ll 1$) this gain vanishes as required for intensity invariant responses whereas the gain (21) asymptotes to s_∞.

References

Baccus, S. A., & Meister, M. (2002). Fast and slow contrast adaptation in retinal circuitry. *Neuron*, *36*, 909–919.

Barlow, H. B. (1961). Possible principles underlying the transformation of sensory messages. In W. Rosenblith (Ed.), *Sensory communication* (pp. 217–234). Cambridge, MA: MIT Press.

Benda, J., & Herz, A. V. M. (2003). A universal model for spike-frequency adaptation. *Neural Computation*, *15*, 2523–2564.

Benda, J., Longtin, A., & Maler, L. (2005). Spike-frequency adaptation separates transient communication signals from background oscillations. *Journal of Neuroscience*, *25*, 2312–2321.

Brenner, N., Bialek, W., & de Ruyter van Steveninck, R. (2000). Adaptive rescaling maximizes information transfer. *Neuron*, *26*, 695–702.

Cartling, B. (1996). A low-dimensional, time resolved and adapting model neuron. *International Journal of Neural Systems*, *7*, 237–246.

Dean, I., Harper, N. S., & McAlpine, D. (2005). Neural population coding of sound level adapts to stimulus statistics. *Nature Neuroscience*, *8*, 1684–1689.

Doolan, J. M., & Pollack, G. S. (1985). Phonotactic specifity of the cricket *Teleogryllus oceanicus*: Intensity-dependent selectivity for temporal parameters of the stimulus. *Journal of Comparative Physiology, A*, *157*, 223–233.

Esch, H., Huber, F., & Wohlers, D. W. (1980). Primary auditory neurons in crickets: Physiology and central projections. *Journal of Comparative Physiology, A*, *137*, 27–38.

Fairhall, A. L., Lewen, G. D., Bialek, W., & de Ruyter van Steveninck, R. R. (2001). Efficiency and ambiguity in an adaptive neural code. *Nature*, *412*, 787–792.

Fourcaud-Trocmé, N., Hansel, D., van Vreeswijk, C., & Brunel, N. (2003). How spike generation mechanisms determine the neuronal response to fluctuating inputs. *Journal of Neuroscience*, *23*, 11628–11640.

French, A. S., Höger, U., Sekizawa, S. I., & Torkkeli, P. H. (2001). Frequency response functions and information capacities of paired spider mechanoreceptor neurons. *Biological Cybernetics*, *85*, 293–300.

French, A. S., & Torkkeli, P. H. (1994). The time course of sensory adaptation in the cockroach tactile spine. *Neuroscience Letters*, *178*, 147–150.

Fuhrmann, G., Markram, H., & Tsodyks, M. (2002). Spike frequency adaptation and neocortical rhythms. *Journal of Neurophysiology*, *88*, 761–770.

Gabbiani, F., & Krapp, H. G. (2006). Spike-frequency adaptation and intrinsic properties of an identified, looming-sensitive neuron. *Journal of Neurophysiology*, *96*, 2951–2962.

Gabbiani, F., Krapp, H. G., Hatsopoulos, N., Mo, C. H., Koch, C., & Laurent, G. (2004). Multiplication and stimulus invariance in a looming-sensitive neuron. *Journal of physiology Paris*, *98*, 19–34.

Hennig, R. M. (1988). Ascending auditory interneurons in the cricket *Teleogryllus commodus* (Walker): Comparative physiology and direct connections with afferents. *Journal of Comparative Physiology, A*, *163*, 135–143.

Hennig, R. M. (2003). Acoustic feature extraction by cross-correlation in crickets? *Journal of Comparative Physiology, A*, *189*, 589–598.

Hennig, R. M., & Weber, T. (1997). Filtering of temporal parameters of the calling song by cricket females of two closely related species: A behavioural analysis. *Journal of Comparative Physiology A*, *180*, 621–630.

Horseman, G., & Huber, F. (1994a). Sound localisation in crickets I: Contralateral inhibition of an ascending auditory interneuron (AN1) in the cricket *Gryllus bimaculatus*. *Journal of Comparative Physiology, A*, *175*, 389–398.

Horseman, G., & Huber, F. (1994b). Sound localisation in crickets II: Modelling the role of a simple neural network in the prothoracic ganglion. *Journal of Comparative Physiology, A*, *175*, 399–413.

Huber, F., Moore, T. E., & Loher, W. (1989). *Cricket behavior and neurobiology.* Ithaca, NY: Cornell University Press.

Kim, K. J., & Rieke, F. (2003). Slow Na^+ inactivation and variance adaptation in salamander retinal ganglion cells. *Journal of Neuroscience*, *23*, 1506–1516.

Knight, B. W. (1972). Dynamics of encoding in a population of neurons. *Journal of General Physiology*, *59*, 734–766.

Kvale, M. N., & Schreiner, C. E. (2004). Short-term adaptation of auditory receptive fields to dynamic stimuli. *Journal of Neurophysiology*, *91*, 604–612.

Laughlin, S. B. (1989). The role of sensory adaptation in the retina. *Journal of Experimental Biology*, *146*, 39–62.

Maravall, M., Petersen, R. S., Fairhall, A. L., Arabzadeh, E., & Diamond, M. E. (2007). Shifts in coding properties and maintenance of information transmission during adaptation in barrel cortex. *PLoS Biology*, *5*(2), e19.

Marsat, G., & Pollack, G. S. (2005). Effect of the temporal pattern of contralateral inhibition on sound localization cues. *Journal of Neuroscience*, *25*, 6137–6144.

Nelken, I., Fishbach, A., Las, L., Ulanovsky, N., & Farkas, D. (2003). Primary auditory cortex of cats: Feature detection or something else? *Biological Cybernetics*, *89*, 397–406.

Nelson, M. E., Xu, Z., & Payne, J. R. (1997). Characterization and modeling of P-type electrosensory afferent responses to amplitude modulations in a wave-type electric fish. *Journal of Comparative Physiology, A*, *181*, 532–544.

Park, T. J., Klug, A., Holinstat, M., & Grothe, B. (2004). Interaural level difference processing in the lateral superior olive and the inferior colliculus. *Journal of Neurophysiology*, *92*, 289–301.

Pollack, G. S. (1988). Selective attentiion in an insect auditory neuron. *Journal of Neuroscience*, *8*, 2635–2639.

Pollack, G. S., & El-Feghaly, E. (1993). Calling song recognition in the cricket *Teleogryllus oceanicus*: Comparison of the effects of stimulus intensity and sound spectrum on selectivity for temporal patterns. *Journal of Comparative Physiology, A*, *171*, 759–765.

Press, W. H., Teukolsky, S. A., Vetterling, W. T., & Flannery, B. P. (1992). *Numerical recipes in C* (2nd edn.). Cambridge: Cambridge University Press.

Reinagel, P. (2001). Neurobiology: The many faces of adaptation. *Nature*, *412*, 776–777.

Römer, H., & Krusch, M. (2000). A gain-control mechanism for processing of chorus sounds in the afferent auditory pathway of the bushcricket *Tettigonia viridissima* (Orthoptera; Tettigoniidae). *Journal of Comparative Physiology, A*, *186*, 181–191.

Sanchez-Vives, M. V., Nowak, L. G., & McCormick, D. A. (2000). Membrane mechanisms underlying contrast adaptation in cat area 17 in vivo. *Journal of Neuroscience*, *20*, 4267–4285.

Schildberger, K. (1984). Temporal selectivity of identified auditory neurons in the cricket brain. *Journal of Comparative Physiology A*, *155*, 171–185.

Schildberger, K., & Hörner, M. (1988). The function of auditory neurons in cricket phonotaxis. *Journal of Comparative Physiology, A*, *163*, 621–631.

Smirnakis, S. M., Berry, M. J., Warland, D. K., Bialek, W., & Meister, M. (1997). Adaptation of retinal processing to image contrast and spatial scale. *Nature*, *386*, 69–73.

Sobel, E. C., & Tank, D. W. (1994). In vivo Ca^{2+} dynamics in a cricket auditory neuron: An example of chemical computation. *Science*, *263*, 823–826.

Solomon, S. G., Peirce, J. W., Dhruv, N. T., & Lennie, P. (2004). Profound contrast adaptation early in the visual pathway. *Neuron*, *42*, 155–162.

Ulanovsky, N., Las, L., Farkas, D., & Nelken, I. (2004). Multiple time scales of adaptation in auditory cortex neurons. *Journal of Neuroscience*, *24*, 10440–10453.

Wang, X. J. (1998). Calcium coding and adaptive temporal computation in cortical pyramidal neurons. *Journal of Neurophysiology*, *79*, 1549–1566.

Weber, T., Thorson, J., & Huber, F. (1981). Auditory behaviour of the cricket I dynamics of compensated walking and discrimination paradigms on the kramer treadmill. *Journal of Comparative Physiology A*, 141, 215–232.

Wiskott, L. (2003). Slow feature analysis: A theoretical analysis of optimal free responses. *Neural Computation*, *15*, 2147–2177.

Wohlers, D. W., & Huber, F. (1982). Processing of sound signals by six types of neurons in the prothoracic ganglion of the cricket, *Gryllus campestris* L. *Journal of Comparative Physiology A*, *146*, 161–173.

Xu, Z., Payne, J. R., & Nelson, M. E. (1996). Logarithmic time course of sensory adaptation in electrosensory afferent nerve fibers in a weakly electric fish. *Journal of Neurophysiology*, *76*, 2020–2032.